FLOW CAMBRIDGE
UNIVERSITY PRESS

RESEARCH ARTICLE

Virus transmission by aerosol transport during short conversations

Rohit Singhal[1],[†] , S. Ravichandran[2],[*],[†] , Rama Govindarajan[3] and Sourabh S. Diwan[1],[*],[†]

[1]Department of Aerospace Engineering, Indian Institute of Science, Bengaluru, KA 560012, India
[2]Nordic Institute for Theoretical Physics, KTH Royal Institute of Technology and Stockholm University, Stockholm 10691-SE, Sweden
[3]International Centre for Theoretical Sciences, Tata Institute of Fundamental Research, Bengaluru, KA 560089, India
*Corresponding author. E-mails: ravichandran@su.se, sdiwan@iisc.ac.in
[†]These authors contributed equally to the work.

Abstract

The SARS-CoV-2 is transmitted not only through coughing, but also through breathing, speaking or singing. We perform direct numerical simulations of the turbulent transport of potentially infectious aerosols in short conversations, involving repetitive phrases separated by quiescent intervals. We estimate that buoyancy effects due to droplet evaporation are small, and neglect them. A two-way conversation is shown to significantly reduce the aerosol exposure compared with a relative monologue by one person and relative silence of the other. This is because of the 'cancelling' effect produced by the two interacting speech jets. Unequal conversation is shown to significantly increase the infection risk to the person who talks less. Interestingly, a small height difference is worse for infection spread, due to reduced interference between the speech jets, than two faces at the same level. For small axial separation, speech jets show large oscillations and reach the other person intermittently. We suggest a range of lateral separations between two people to minimize transmission risk. A realistic estimate of the infection probability is provided by including exposure through the eyes and mouth, in addition to the more common method of using inhaled virions alone. We expect that our results will provide useful inputs to epidemiological models and to disease management.

Impact Statement

Asymptomatic transmission, through activities like speaking, is believed to be an important route of COVID-19 spread across the world. The evolving turbulent jet that emerges from the mouth of a speaker can carry aerosols to large distances. While direct numerical simulations of turbulent speech flow are becoming common, very little is understood about two-way conversations. We simulate these to obtain spatiotemporal distributions of aerosols and calculate infection probabilities. We show that the interaction between the two speech jets plays a key role in determining this probability. The risk of infection is reduced considerably during a 'dialogue' as compared with a 'monologue' and a small height difference is found to be more dangerous than the two speakers being of equal heights. The present results can inform public health guidelines for minimizing risk of transmission, such as introducing a lateral separation between conversing people, among other measures.

CrossMark

1. Introduction

The SARS-CoV-2, responsible for the COVID-19 pandemic, is known to be transmitted through more than one mode. During the early days of the pandemic (in early 2020), the primary mode of infection was believed to be through droplet transmission by an infected symptomatic person, through violent expiratory events like coughing. Based on this, the World Health Organisation recommended maintaining a physical distance of 1 m between people to minimize the spread of infection, whereas the recommendation of the United States Centers for Disease Control and Prevention is a separation of 6 ft (approximately 1.8 m). By the middle of 2020, it was clear that asymptomatic transmission of the virus was equally likely, through the virus-laden droplets released by an infected person while talking, singing, breathing, etc. (Asadi, Bouvier, Wexler, & Ristenpart, 2020a; Morawska & Cao, 2020), and that this could potentially cause a rapid spread of the disease. This led to the realization that public health measures such as mask wearing and physical distancing would be necessary in ordinary situations since an infected person (symptomatic or asymptomatic) who merely engaged in a conversation could spread the disease (Asadi et al., 2020a). More recently, the airborne transmission of virus driven by background air currents, such as ventilation, has been found to be responsible for the spread of SARS-CoV-2 in indoor settings. These findings highlight the need to better understand the different transmission modes of SARS-CoV-2, in which the fluid dynamics of droplet/aerosol transport plays a key role (Bourouiba, 2021). In particular, scientific attention has been focused on the physical distancing guidelines as set out in public health advisories, which were based at first on a study done in the 1930s (Wells, 1934). According to that study, large droplets ($>100\,\mu m$) settle faster than they evaporate but can cover ≈ 1 m horizontally while doing so, causing direct transmission. It was estimated that smaller droplets cannot directly transmit the disease due to their fast evaporation. Recent research has shown that smaller droplets can cause disease as well. There is an entire spectrum of droplet sizes released during different expiratory events, and a significant part of this size spectrum can be transported over long distances by the turbulent jet/puff generated during such events (Bourouiba, 2021). The respiratory turbulent jet further contains water vapour which slows down evaporation. The complexity of the transmission dynamics of SARS-CoV-2, coupled with its asymptomatic transmissibility, could thus have played a large role in the ongoing pandemic afflicting the world (Prather, Wang, & Schooley, 2020), with several countries experiencing third or fourth waves of the contagion at present.

Bourouiba (2021) discusses the break-up of mucosalivary fluid bubbles and the formation of droplets ranging from 1 to $500\,\mu m$ (Duguid, 1946; Johnson et al., 2011) during different expiratory events. In this range, the large virus-laden droplets predominantly cause direct transmission or contaminate surfaces close to their source (Basu, Kabi, Chaudhuri, & Saha, 2020; Bhardwaj & Agrawal, 2020) turning them into 'fomites'. Small droplets can stay airborne for longer times, their longevity being a function of their composition as well as prevalent ambient conditions such as the relative humidity and temperature. Furthermore, small droplets can evaporate completely while airborne and turn into what are called droplet nuclei. The SARS-CoV-2 has been found to survive in aerosols (typically consisting of microdroplets and droplet nuclei of sizes less than $5\,\mu m$) with a half-life of approximately 15 minutes for typical indoor conditions (Marr, Tang, Van Mullekom, & Lakdawala, 2019; Schuit et al., 2020; US Department of Homeland Security, 2020); another study (Van Doremalen et al., 2020) found the virus half-life in aerosols to be 1.1 hours (Greenhalgh et al., 2021). The long-range transport of disease-causing viruses through such droplets and droplet nuclei, and the impact of the ambient conditions on virus survival, are open questions of fluid dynamical interest (Bourouiba, 2020), with some studies suggesting that droplets with diameters in the range of (2.5–$19\,\mu m$) have the greatest potential for causing the initial nasopharyngeal infection (Basu, 2021; Smith et al., 2020). Droplets exhaled while speaking are typically smaller than $10\,\mu m$ (Asadi et al., 2019) and lie in the described range for higher nasopharyngeal infection.

Most of the fluid dynamical studies on human expiratory flows have focused on droplet transport during coughing and sneezing, due to their direct relevance to symptomatic transmission. Several

experimental (Bourouiba, Dehandschoewercker, & Bush, 2014; Clark & De Calcina-Goff, 2009; Gupta, Lin, & Chen, 2009; Nielsen, Olmedo, De Adana, Grzelecki, & Jensen, 2012; Tang, Liebner, Craven, & Settles, 2009; Wei & Li, 2017) and numerical (Balachandar, Zaleski, Soldati, Ahmadi, & Bourouiba, 2020; Dbouk & Drikakis, 2020; Fabregat et al., 2021; Liu, Allahyari, Salinas, Zgheib, & Balachandar, 2021; Liu, Li, Nielsen, Wei, & Jensen, 2017; Qian & Li, 2010; Rosti, Cavaiola, Olivieri, Seminara, & Mazzino, 2021; Rosti, Olivieri, Cavaiola, Seminara, & Mazzino, 2020; Wang et al., 2021) studies of cough and sneeze flows have been reported and their outcomes are being incorporated into epidemiological models (Chaudhuri, Basu, & Saha, 2020; Dbouk & Drikakis, 2021). On the other hand, the fluid dynamics of speech and breathing has received much less attention until very recently. Shao et al. (2021) provide a risk assessment of virions exhaled due to normal breathing in elevators, classrooms and supermarket settings. Chong et al. (2021) carried out a direct numerical simulation (DNS) of a turbulent vapour puff and found that droplets can last $O(100)$ times longer in cold humid air than predicted by classical models (Wells, 1934); they used an inlet flow rate profile typical of a cough but the results are equally applicable to other expiratory flows including speech. Recent experiments (Giovanni et al., 2021) on the effects of airflow velocity on droplet trajectory in speech and vocal exercises have been used to construct models of the behaviour of different droplets. Abkarian, Mendez, Xue, Yang, and Stone (2020) carried out a large eddy simulation of speech flows generated by the repetition of certain phrases. They showed that beyond a certain distance from the mouth of the speaker, speech flow behaves like a steady jet that spreads at a typical half-angle of $10°$. These results were incorporated by Yang, Pahlavan, Mendez, Abkarian, and Stone (2020) into a simplified model for the transport of aerosol particles away from a speaker's mouth, using known properties of steady jets such as the $1/x$ variation of the velocity and scalar concentration with the axial distance x. They calculated the probability of infection of a silent listener based on conservative estimates of the minimum number of virions ($N_{inf} \approx 100$) that must be inhaled to cause infection (Basu, 2021; Kolinski & Schneider, 2020) and presented space–time maps of the risk of infection. This study highlighted the fact that the disease transmission by speech involves not just distances but also exposure times (see also Tan, Silwal, Bhatt, and Raghav (2021)) and that these should also be incorporated in the public health guidelines.

The idealized scenario studied in Abkarian et al. (2020) and Yang et al. (2020), where a single person engages in an extended monologue, is of limited applicability, and typical public interactions are dialogues of short time spans, e.g. over-the-counter conversations at a supermarket. The present study is devoted to gauging infection probability from such a short, unmasked conversation between two people, by performing a DNS of speech flow. We compute turbulent transport of speech aerosols, which play a key role in the transmission of virus. We estimate the total viral ingestion by a listener by including exposure through the eyes and mouth, in addition to the aerosols inhaled through the nose (more commonly only the last is used to determine viral dose). We show that the active participation in the conversation of the second person significantly alters the evolution of the jet from the first person, dramatically mitigating infection probability. Any temporal asymmetry in speech enhances the risk of infection to the person who speaks less. Secondly and rather interestingly, a small vertical or lateral separation between the mouths of the speakers actually increases the infection probability, due to a less effective interference of the two jets. At large vertical or lateral separation, infection probability is lower, as would be expected. We discuss the implications of these results for improving physical distancing guidelines and for epidemiological modelling. Also, our results offer interesting experimental test cases and can be used to validate flow-modelling approaches such as the Reynolds-averaged Navier–Stokes equations.

At the time of preparing a revision to this paper, we came across a very similar computational study carried out by Giri et al. (2022). (They have also reported results from idealized laboratory experiments.) While their conclusions are broadly consistent with ours, we have carried out a more detailed calculation of infection probabilities for a variety of speech scenarios and done more extensive simulations. More comments are made in the following sections.

The paper is organized as follows. First, we describe the computational geometry and set-up (§ 2), followed by the parameters needed to estimate the infection risk. We present two cases: one in which

one of the people is a passive listener, and the other in which both people converse. Next, we describe our method of determining the total exposure and ingestion of virions, which is used to calculate the probability of infection for the above two cases; we also analyse a case with temporal asymmetry in speech duration (§ 3). Lastly, a discussion of our results, including their implications towards devising public health guidelines is presented (§ 4), before summarizing the findings in § 5.

2. Numerical experiments

2.1. *Computational set-up and parameters of simulation*

We use two types of computational domain for the DNS of speech flows. The first type of simulation, case I, is done using a domain whose side view is shown in figure 1(a) (the lateral size of the domain is the same as that shown in figure 1b); the coordinate system used is shown in the figure. Here, a silent susceptible listener is prescribed at $(L_s, y_s, z = 0)$ with respect to the origin 'O' where the speaker (person 1) is placed. A circular region of interest (ROI) of diameter 17.2 cm (which is approximately the diameter of a human face) is used to represent the face of person 2 (figure 1a). To examine the 6 ft (approximately 1.8 m) rule, the length of the computational domain is chosen to be $L_x = 1.96$ m, and the vertical and lateral extents are chosen to be $L_y = L_z = 0.98$ m which are sufficient for the study due to the small spread angle ($\approx 20°$–$28°$) of speech flows (Yang et al., 2020). The grid resolution used is $256 \times 128 \times 128$ in $L_x \times L_y \times L_z$, which is equivalent to 256^3 for a cubical domain with size L_x. As done in previous studies (Ravichandran & Narasimha, 2020; Singhal, Ravichandran, Diwan, & Brown, 2021), open boundary conditions are imposed on the four lateral boundaries at $y = -L_y/2, L_y/2$ and $z = -L_z/2, L_z/2$ and the boundary at $x = L_x$; this enables advection of the turbulent structures out of the domain, without affecting the upstream flow. A free-slip condition is used for the boundary at $x = 0$, except for the orifice at 'O' (see below).

Case II is a set of simulations where the two people are in conversation (figure 1b), and the flows thus generated interact with each other. We account for a possible height difference between the speakers by a vertical separation y_s. The orifice for person 1 is located at $(0, 0.5 \times y_s, 0)$ and that for person 2 (whose susceptibility to infection is being estimated) at $(L_s + \Delta, -0.5 \times y_s, 0)$, as shown schematically in figure 1(b). To account for the obstacle created by person 2 to the incoming speech flow for this case, the boundary at $x = L_x = (L_s + \Delta)$, excluding the orifice, is prescribed to be a free-slip wall (instead of an outflow boundary) similar to that at $x = 0$. In order to avoid wall effects, we choose an axial location that is at a distance $\Delta (\approx 0.15$ m) upstream of L_x to place the ROI. The use of the free-slip boundary condition, as compared with the outflow boundary condition, is found to have an insignificant effect on the scalar flux reaching person 2 (see figure S2 in the supplementary material). The axial length of domain is varied among three values, $L_s \in \{0.6, 1.2, 1.8$ m$\}$, keeping the lateral lengths $L_y = L_z = 0.98$ m fixed. The grid resolution used for $L_s = 0.6$ m is 128^3, whereas that used for the other two values of L_s is $256 \times 128 \times 128$. Our results are largely insensitive to the grid resolution, as we show in § 2.2. We also wish to understand the rate of infection when the conversation is temporally asymmetric, i.e. person 1 speaks more than person 2. We simulate such situations with $L_s = 1.2$ m and $y_s = 0$ and name it 'case IIt'.

The speaker's mouth is modelled as an elliptical orifice with half-axis dimensions of $a = 1.5$, $b = 1.0$ cm, following Abkarian et al. (2020). We use the characteristic diameter $d = 2\sqrt{ab} = 2.45$ cm of the ellipse as the length scale for non-dimensionalization; the non-dimensional size of the domain is therefore ($80d \times 40d \times 40d$) for $L_s = 1.8$ m. Similarly, the other domain sizes are $L_s = 1.2$ m $= 55d$ and 0.6 m $= 30d$. Prescribing speech flow at the orifice is not straightforward as it involves complex linguistic expression, which can continue for an extended period of time. Here we follow Abkarian et al. (2020) in choosing a simple repetitive phrase for simulating speech flow. Abkarian et al. (2020) show that speech phrases with plosive sounds (e.g. words containing the letter 'P' – *Oshtavya* in Sanskrit) induce puffs that travel farther than those having fricative sounds (e.g. the letter 'S'). Furthermore, the speech jet produced by plosives was found to be directed primarily in the axial direction (Abkarian et al., 2020), obviating the need to introduce flow directionality at the orifice. We therefore use a repeated
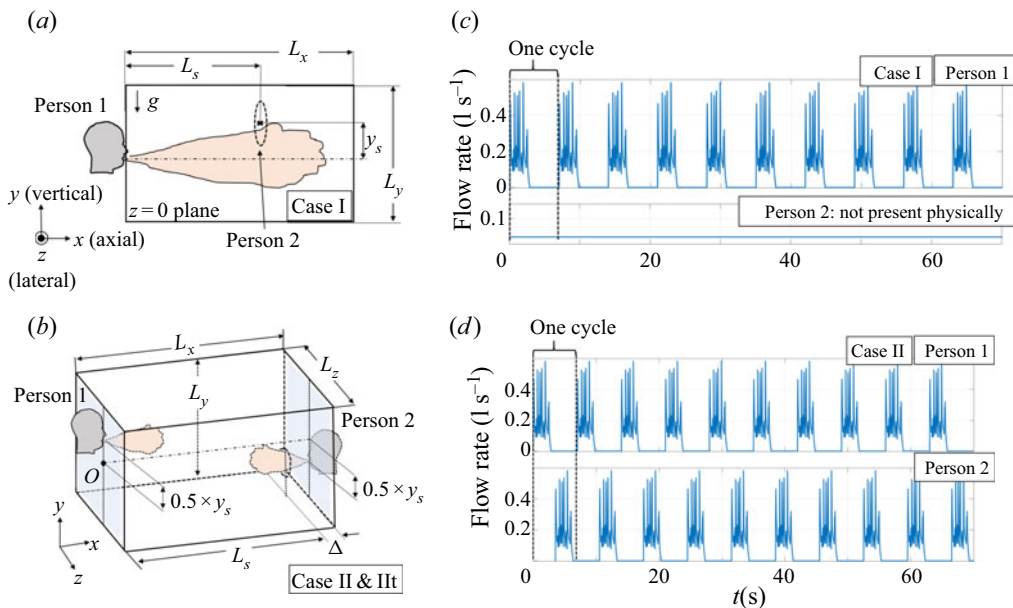
Figure 1. *(a) Side view ($z = 0$) of the computational domain in case I showing the location (L_s, y_s) of the silent (and susceptible) listener, represented by a circular ROI as shown in the figure. (b) Three-dimensional representation of the computational domain in case II, where both person 1 and person 2 speak, and L_s and y_s are treated as parameters. The orifices are displaced symmetrically about $y = 0$. (c) Inlet flow rate (in l s^{-1}) from the orifice 'O' in case I. (d) Inlet flow rates from the two orifices in case II.*

utterance of the phrase 'Peter Piper picked a peck' and prescribe the inlet velocity at the orifice (in the axial direction) using laboratory measurements of flow velocity associated with this phrase (see figure 4c of Abkarian et al., 2020). In Abkarian et al. (2020) consecutive speech phrases are separated by inhalation through the mouth. For simplicity, we do not include the inhalation part of the speech cycle in our simulations (see supplementary material, § 1 for more details on numerical issues). Abkarian et al. (2020) anticipated that this would not affect the transport of aerosols except in a region very close to the mouth. To confirm this, we have carried out a detailed analysis of the effect of inhalation, of both speaker and listener, on the flow pattern and on the total aerosol exposure on person 2. The results of this exercise are presented in the supplementary material, § 1. As seen from figures S2, S3, S5 and S6 (see supplementary material), the inclusion of inhalation in the speech cycle has a negligibly small effect on the scalar transport away from the speaker and can safely be excluded in estimating the viral load of infected aerosols to the listener. While inhalation by the listener does curve the streamlines in the region close to the mouth, this has no effect on our findings since we estimate infection by the aerosol load on the entire face. In the present study, the exhalation phase of the phrase has a volume of 0.5 litre per cycle (Abkarian et al., 2020), which lasts for 2.8 s, followed by a halt in speaking of 4.2 s, which makes one complete cycle of speech (figure 1c,d).

For case I, we have used 10 speech cycles for person 1 and zero flow rate for person 2 (who acts like a silent listener, though not physically present in the domain); see figure 1(a,c). For the simulations in case II, flow rates at both orifices (corresponding to persons 1 and 2) consist of 10 staggered cycles shown in figure 1(d); this represents each person taking turns to speak the same phrase. In case IIt, person 1 and person 2 have 10 cycles of conversation, following which, person 2 stops speaking, and person 1 continues for another 10 cycles (see § 3.4). For this case, the total speech time (including the silent intervals) is 140 s for person 1 and 70 s for person 2. The maximum flow velocity at the orifice, $u_c = 1.167$ m s^{-1}, is used as the velocity scale for all the cases. Since these flow speeds are small

compared with the speed of sound in air and also because the change in density within the flow is much smaller than the ambient density ($|\varDelta\rho|/\rho \approx 0.05$ for $\Delta T = 14\,°C$ at the orifice; see appendix A) we may make the Boussinesq approximation. This involves treating the velocity field as effectively incompressible with the density differences relevant only for the buoyancy term in the momentum equation. The buoyancy module of our code has been validated for a steady plume (Singhal et al., 2021) wherein the self-similar decay of the centreline temperature has been accurately captured. For the speech flows considered here, it turns out that the buoyancy forces are much smaller than the inertia forces. As a result, the flow does not show any perceptible deflection in the vertical direction on average (figure S13 (supplementary material)) and is qualitatively similar to that reported in Abkarian et al. (2020) who did not solve for temperature. This is borne out by the small value of Fr^{-2} (= 0.00842) obtained for the present simulations based on the orifice conditions, where Fr is the Froude number (appendix A). Furthermore, the temperature drops rapidly as the speech jet issues from the orifice (by approximately $10\,°C$ over 0.5 m from the orifice; see figure S14 (supplementary material)) and remains ineffective compared with flow momentum to bring about any noticeable change in the flow trajectory over the present simulation time.

In order to model the dynamics of virus-laden droplets generated during speech, we make two simplifications. First, that most droplets ($O(10\,\mu m)$ or less) produced during speech are small enough that they follow fluid streamlines. The smallness can be quantified in terms of the Stokes number of the droplets, defined as the ratio τ_p/τ_f, where τ_p is the time scale on which the velocity of a droplet adjusts itself to the local fluid velocity, and $\tau_f = d/u_c$ is the flow time scale. For droplet sizes typical of speech flows, Stokes numbers are much smaller than unity (Yang et al., 2020), which means that within a fraction of the flow time scale, a droplet attains the same velocity as the flow. In other words, it behaves as a passive scalar. In the present work, $\tau_p \sim 0.5$ ms (for $10\,\mu m$ droplets) and $\tau_f \sim 20$ ms, giving $\tau_p/\tau_f \sim 0.025$ which is much less than unity; for smaller droplets τ_p/τ_f is even smaller. Since the flow velocity rapidly drops away from the orifice, the passive-scalar approximation is justified in the entire domain. This approach has been used before for studying the interaction of droplets and turbulence in a cloud flow (Ravichandran & Narasimha, 2020) and allows us here to represent small droplets in speech flow by scalar fields of concentration C_{s1} and C_{s2} emanating from persons 1 and 2, respectively (for case I, $C_{s2} = 0$).

We prescribe unit concentration at the orifices during speaking and zero otherwise. We note that the total liquid content in these flows is quite small and a vast majority of droplets are $5\,\mu m$ or smaller (Asadi et al., 2019). Netz (2020) found that the time taken by a speech droplet of diameter $10\,\mu m$ to evaporate completely is approximately 0.1 s at an ambient relative humidity of 50%, and smaller droplets will evaporate faster. Even at the high end of expected humidity levels, a $10\,\mu m$ diameter would evaporate over time of the order of 1 s (see e.g. Chong et al., 2021). The typical distance travelled in 1 s is only approximately 0.2 m for case I, i.e. when the listener is silent (figure S8 (supplementary material); see also Giri et al. (2022)). During conversations, this distance is much shorter. Thus even in the worst-case scenario, and even when the distance between the people is only 2 ft (approximately 0.6 m), we can expect all the droplets to have evaporated (turning into dried droplet nuclei) before the aerosols reach the other person. On the other hand, the typical half-life of SARS-CoV-2 in speech droplets/nuclei is 15 minutes to 1 hour (Schuit et al., 2020; Van Doremalen et al., 2020). Thus it is the dried nuclei that act as effective carriers of the virus, much after the liquid droplets have completely evaporated. Moreover, the effect of evaporation on flow buoyancy has been shown to be negligibly small by Chong et al. (2021). In their moist-cough simulations, they included buoyancy due to evaporating droplets of size ranging from 10 to $1000\,\mu m$ but did not observe any perceptible deflection of the cough flow. Ng et al. (2021) have reported the typical temperature differences induced by droplet evaporation to be approximately $2\,°C$ for an initial diameter of $15\,\mu m$, which is the worst-case scenario for speech droplets. For the present speech flow, we find temperature differences to be approximately $7\,°C$ for $x < 0.5$m and less than $4\,°C$ for $x > 0.5$ m (figure S14 (supplementary material)), but do not observe any vertical deflection of the flow as mentioned above (figures S13, S14 (supplementary material)). We thus anticipate any additional buoyancy effects due to droplet evaporation to be negligible for our speech flow. We therefore do not

incorporate the thermodynamics of evaporation in this study, and treat small droplets and droplet nuclei as interchangeable; we refer to both as 'aerosols'. This is consistent with Abkarian et al. (2020), Yang et al. (2020) and Giri et al. (2022), who have not considered effects of droplet evaporation in their speech-flow simulation/modelling. The resulting governing equations, namely the Boussinesq–Navier–Stokes equations, the continuity equation and the scalar transport equations, are solved using the finite volume DNS solver, Megha-5 (for further details, see appendix A).

2.2. *Grid resolution and validation*

To assess the effect of grid size on the simulation results, we have carried out a detailed grid-resolution exercise, which is presented in supplementary material, § 2. The exercise is performed in two parts. First, to examine the behaviour of the cycle-averaged velocity, we use a cubical domain of $70d^3$ and carry out simulations for three grid resolutions: 1024^3, 512^3 and 256^3. The speech cycle used is similar to that used in Abkarian et al. (2020), except for the inhalation. The cycle-averaged velocity as a function x is plotted in figure S7(a–c) (supplementary material) for each of these simulations. Figure S7(d) (supplementary material) presents a comparison among the three resolutions which shows no significant effect on the findings (see the caption of figure S7 (supplementary material) for more specific comments). Importantly, the cycle-averaged centreline velocity reproduces the $1/x$ variation after $x \approx 0.4$ m typical of a steady jet, as reported in Abkarian et al. (2020). Note that the departures from the $1/x$ behaviour for $x < 0.4$ and $x > 1$–1.4 m (depending upon the cycle number used for averaging) are similar to those observed in Abkarian et al. (2020) for their speech phrase (their figure 5d). We also find (using a somewhat different domain size) that the 'flow length' exhibits the $t^{1/4}$ variation for small t (typical of a 'puff'), followed by the $t^{1/2}$ variation at large t (typical of a 'starting jet') as obtained in Abkarian et al. (2020) (figure S8a (supplementary material)). Note that the $t^{1/4}$ variation is seen over only a short period, since the simulated speech flow consists of a series of puffs (rather than a single puff), which merge together to form a 'starting jet' after a short time and a short downstream distance; over an intermediate range of distances this jet exhibits the quasi-steady behaviour seen in figure S7 (supplementary material). The results in figures S7 and S8(a) (supplementary material) serve as a validation of our results against those of Abkarian et al. (2020).

In the second part of the grid-resolution exercise, we take a closer look at the effect of varying grid size on the behaviour of velocity fluctuations. This is important since turbulence has an important role to play in the dynamics and evolution of respiratory flows (Rosti et al., 2021). Towards this objective, we carry out simulations for case I (figure 1a) with a domain size of $80d \times 40d \times 40d$ and with two grid resolutions: $256 \times 128 \times 128$ (same as used for the present results) and $512 \times 256 \times 256$ (a finer grid). We calculate the dissipation of turbulence kinetic energy and the Kolmogorov length scale ($\overline{\eta}_K$; see supplementary material, § 2, for details) corresponding to the maximum dissipation rate at a given x and t, which is plotted in figure S9(a,b) (supplementary material). It is evident that both resolutions give nearly the same values of $\overline{\eta}_K$, which is typically 2 mm or larger (except for $x < 0.4$ m and $t < 30$ s; figure S9a,b (supplementary material)). Note that the grid spacing for the resolution of $256 \times 128 \times 128$ is 7.66 mm and that for $512 \times 256 \times 256$ is 3.83 mm for case I. Thus even though our simulation does not resolve the Kolmogorov scale everywhere in the domain, the fact that this scale does not change upon doubling the grid size implies that we capture the energy dissipation rate with a sufficient level of accuracy. This means that our simulation is sufficiently spatially resolved. (See for example Moin and Mahesh (1998) who state that the requirement for a DNS to be 'spatially resolved' is that the dissipation should be captured accurately, and that it is not necessary for the grid size to be as small as the Kolmogorov scale.) As a further support, we compare (figure S9c (supplementary material)) our variation of $\overline{\eta}_K$ over the quasi-steady regime (0.45 m $< x <$ 1.4 m) with that obtained from the measurement of dissipation in a steady round jet by Panchapakesan and Lumley (1993), for a matched Reynolds number (see also Pope (2000)). It is evident from figure S9(c) (supplementary material) that there is an excellent agreement between the two (except for statistical fluctuations). It is worth noting that our grid resolution is better than that used in the DNS of studies on cough flows by Chong et al. (2021) and Rosti et al. (2021) when

adjusted for Reynolds number, since our Reynolds number is much lower than that used in these studies (see table S1 (supplementary material)). While the DNS of conversation by Giri et al. (2022) uses a grid size of 2 mm which is smaller than ours, in view of the above discussion, we see our grid size of $256 \times 128 \times 128$ to be adequate. This exercise serves us well in reducing the computational cost, and enables us to report results from a large number of simulations (nearly 25).

Finally, we compare some of the relevant flow parameters between the two grid resolutions, i.e. $256 \times 128 \times 128$ and $512 \times 256 \times 256$. The length of the flow and its radial extent for case I are compared in figure S8(*a,b*) (supplementary material). The total aerosol exposure on a listener (§ 3.1) and the amount of aerosol within the domain for case I are plotted in figure S10(*a,b*) (supplementary material). We have also simulated one conversation case (case II) with a higher resolution; the time variation of the aerosol flux from this simulation is compared with that from the present resolution of $256 \times 128 \times 128$ in figure S11 (supplementary material). Figure S12 (supplementary material) compares the number of virions ingested by a listener (§ 3.3) for this case as well as that for case I. We find good quantitative agreement between results from the two resolutions (for more comments see supplementary material, § 2), which provides further support to the adequacy of the present resolution. Note that statistical variations, which are inherent between different realizations of a transient jet (with slightly different initial/boundary conditions), are partly responsible for the observed deviations between the two resolutions; see supplementary material, § 2. This feature was also reported in Abkarian et al. (2020).

3. Results

3.1. *Case I: person 1 speaking and person 2 being a silent listener*

Studies (Chaudhuri et al., 2020; Yang et al., 2020) have provided spatial and temporal separation guidelines using calculations based on the total viral load on a susceptible person present at a specific location. The infection probability is then calculated from the number of virions inhaled by the person. However, several studies have found that infections may also be caused by viral contact through other exposed areas, such as the eyes (Chen et al., 2020; Coroneo & Collignon, 2021; Sun, Wang, Liu, & Liu, 2020; Xie et al., 2020) or the mouth and lips (WHO Scientific Brief, 2020). In order to include these possibilities, we estimate the exposure of a listener to virus-laden aerosols over an ROI positioned in front of their face. Towards this, we determine aerosol concentration (ϕ) which is related to the passive scalar concentration as $\phi = \phi_o (C_s/C_{so})$, where ϕ_o represents the volume of droplets (i.e. liquid volume) per unit volume of air at the orifice and $C_{so} = 1$ (see appendix A). The available experimental studies show that the production rates of droplets generated during speech are a function of the loudness of the speech (Asadi et al., 2019; Asadi et al., 2020b; Gregson et al., 2021) with the liquid volume fraction varying in the range 6×10^{-9}–1×10^{-8}, depending upon the loudness. Here we use $\phi_o = 6 \times 10^{-9}$, which is relevant for a 'typical' speech, i.e. with moderate levels of loudness (Yang et al., 2020). Yang et al. (2020) have also used the higher value of $\phi_o = 1 \times 10^{-8}$ in their analysis; see also Giri et al. (2022). The effect of the precise value of ϕ_o on the risk of infection is discussed in § 4.2. As mentioned earlier, the speech droplets evaporate fast and turn into droplet nuclei but the total number of virions carried by the speech aerosols remains the same; see Yang et al. (2020). The flux of aerosols through an ROI centred at $(L_s, y_s, z = 0)$ is given as

$$f(L_s, y_s, t) = \int\int \phi_1 u \, \mathrm{d}y \, \mathrm{d}z; \quad 2\sqrt{(y - y_s)^2 + z^2} < D_{ROI}, \qquad (3.1a,b)$$

where ϕ_1 is the aerosol concentration corresponding to the speech flow of person 1, u is the axial velocity and $D_{ROI} = 17.2$ cm is the diameter of the ROI. The aerosol flux through the ROI is taken as the viral exposure to the face of the listener. Since the deflection of the flow by buoyancy is negligible, the y and z directions are equivalent. We therefore only need to vary L_s and y_s. Figure 2(*a*) shows the time series of the aerosol flux across an ROI for case I, $f_I (L_s, y_s = 0, t)$, using the data obtained from
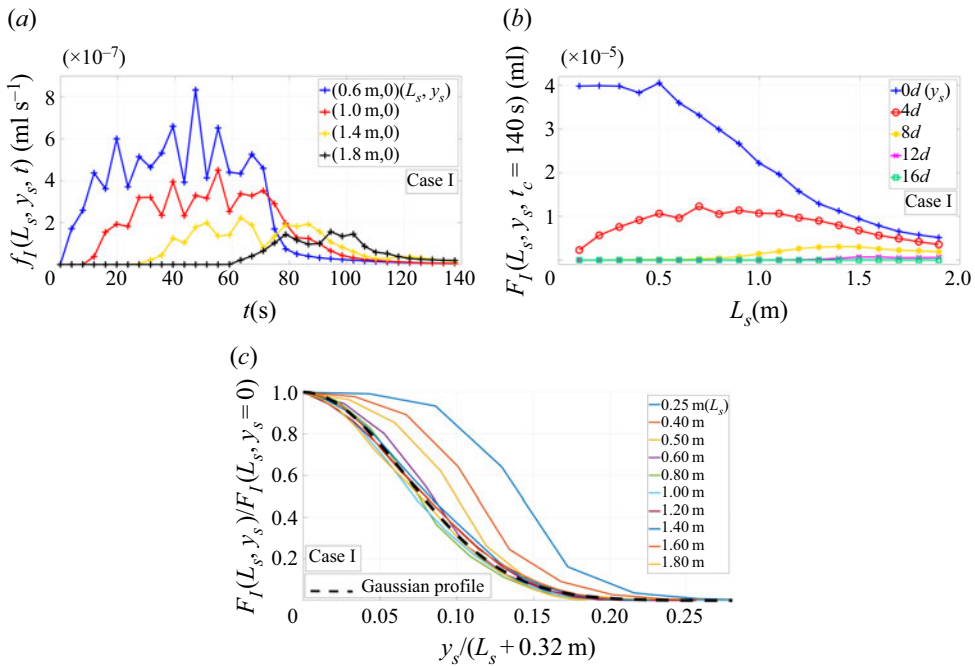
Figure 2. *Aerosol flux for case I. (a) Variation in time of the aerosol flux f_I through the circular ROI centred at $(L_s, y_s = 0)$. Close to the orifice, the flow is resembles a series of puffs rather than a jet. (b) The total scalar exposure $F_I(L_s)$ over the simulation time (140 s), for different height differences y_s. Interestingly, F_I varies non-monotonically with L_s for non-zero y_s. This is because only a part of the speech-flow jet intersects the ROI for $L_s \lesssim 10y_s$. (c) Vertical variation of normalized $F_I(L_s, y_s)$ and its comparison with a Gaussian curve. The normalized F_I profiles show best collapse with a virtual origin at 0.32 m upstream of the orifice.*

the simulations. The transition of the flow from a puff-like behaviour to jet-like behaviour can be seen from the decrease in the oscillations of the scalar flux with increase in L_s. The total aerosol exposure to the listener $F(L_s, y_s, t_c)$ over time t_c is given by the time integral of the aerosol flux through the ROI,

$$F(L_s, y_s, t_c) = \int_0^{t_c} f(L_s, y_s, t)\, \mathrm{d}t, \tag{3.2}$$

where t_c is the duration of exposure and F is units of volume (here millilitres). Here we show results for $t_c = 140$ s (although the total speech duration is 70 s) as this represents the time until which the listener at $L_s = 1.8$ m continues to receive aerosol flux from the speaker (figure 2a,b). The aerosol exposure $F_I(L_s, y_s, 140\,\text{s})$ for case I is plotted in figure 2(b) as a function of axial location L_s at five different vertical locations y_s. For $y_s = 0$, the total exposure is practically constant for $L_s < 0.5$ m, because the area of the ROI is larger than the cross-section of the jet until this axial location. Once the jet cross-section area exceeds the area of the ROI, the total exposure starts decreasing (figure 2b). When the listener is not aligned with the speaker face to face ($y_s \neq 0$), F_I increases with L_s for $L_s \lesssim 10y_s$, before decaying at large L_s.

The vertical profiles of $F_I(L_s, y_s, 140\,\text{s})$ are found to be bell-shaped curves with the peak in F_I decreasing with increase in L_s. Suitably scaled versions of the profiles of F_I are plotted in figure 2(c). The F_I profiles at $L_s = 0.25, 0.40$ and 0.50 m, show an evolution in shape, and show an approach towards a Gaussian distribution (represented by a dashed curve); this is consistent with the observation that flow is in a transition state between a puff and steady jet for these distances. For $L_s > 0.50$ m, the curves

collapse well onto the Gaussian curve (figure 2c). Note that the Gaussian distribution for the scalar flux profiles is typical of a self-similar jet (Turner, 1986). A more commonly used indicator for the start of the self-similar regime is the $1/x$ variation of the centreline scalar concentration. Such a variation starts from $L_s \approx 0.45$ m (figures S7 and S15b (supplementary material)) and we find it convenient to associate this location with the beginning of steady, self-similar speech flow. These results are useful for determining viral exposure to the listener's eyes and mouth, as will be seen.

We first obtain a conservative estimate of the aerosol flux inhaled by a listener by using the fact that the domain of inhalation is much more localized than has been considered in some of the previous studies. In particular, Yang et al. (2020) have used a measure of aerosol concentration (Φ_H) that is averaged over an area with radius $r_H = x \tan \alpha$, where the half-cone angle α encompasses 90 % of scalar within it. These effectively represent 'top-hat' quantities and therefore have been denoted by a subscript 'H'. Using this formulation, Yang et al. estimated the number of inhaled virions as

$$N(\Phi_H) = c_v \Phi_H(x) Q_r t = c_v \phi_o a_H Q_r t / (x \tan \alpha), \qquad (3.3)$$

where c_v is the number of virions per unit droplet volume (or the total saliva volume) in the exhaled air during speech, a_H is the orifice radius and Q_r is the average rate of inhalation by the listener taken as $0.1 \, \mathrm{l \, s^{-1}}$. However, the actual distributions of axial velocity and scalar concentration in a steady self-similar jet are Gaussian, and it is therefore of interest to relate r_H and Φ_H with their Gaussian counterparts. The relevant length scale characterizing a Gaussian distribution is the '$1/e$ width' (b_e), defined as a radial distance where a quantity reaches $1/e$ times its centreline value – for axial velocity we denote it as $b_{ue}(x)$ and for aerosol concentration as $b_{\phi e}(x)$. The centreline values of the mean axial velocity and aerosol concentration are denoted as $U_c(x)$ and $\phi_c(x)$, respectively. We get the relation between the top-hat width of Yang et al. (2020) and the Gaussian widths as $r_H = 1.516 b_{\phi e}(x) = 1.819 b_{ue}(x)$ (see supplementary material, § 4). Thus, the top-hat radius considerably overestimates the lateral spread of the aerosol distribution. As a result of this, the top-hat velocity ($U_H(x)$) and aerosol concentration ($\Phi_H(x)$) are underestimated in relation to their Gaussian counterparts as $U_H(x) = 0.39 U_c(x)$ and $\Phi_H(x) = 0.462 \phi_c(x)$; (see figure S15 (supplementary material) for a graphical comparison). Thus, a susceptible listener can be expected to get exposed to a larger number of virions than estimated in Yang et al. (2020). To make a realistic estimate of the aerosol flux inhaled by a listener, we consider inhalation to be a 'sink' flow (with nose at its centre), drawing in air from a hemispherical domain with a radius of 6.2 cm (Abkarian et al., 2020; Haselton & Sperandio, 1988). An average aerosol concentration is then calculated over this localized circular region centred at the jet axis (rather than over the much larger area, πr_H^2) given as

$$\Phi_{new} = (b_{\phi e}/6.2)^2 [1 - \exp(-(6.2/b_{\phi e})^2)] \phi_c, \qquad (3.4)$$

which represents the average scalar concentration a listener is likely to ingest through the inhalation process; here $b_{\phi e}$ is measured in centimetres (for derivation, see supplementary material, § 5). Using $\Phi_H(x) = 0.462 \phi_c(x)$ and $b_{\phi e} = 0.137 x$ for a steady self-similar jet (Singhal et al., 2021), we obtain a relation between Φ_{new} and Φ_H as a function of x. This is plotted in figure 3, which shows that $\Phi_{new} > \Phi_H$ for $x > 0.45$ m; the region up to this axial location is shown shaded as the Gaussian profile does not apply in this region. The figure also shows that for $x > 1$ m, $\Phi_H(x) \approx 0.5 \Phi_{new}(x)$; the use of the top-hat profile thus underestimates the risk of infection by direct inhalation of virions by approximately 50 %, supporting our expectation mentioned earlier.

3.2. Case II: persons 1 and 2 engaged in conversation

Thus far, the listener was entirely passive. In this set of simulations (case II), person 2 is present at a location $L_x = L_s + \Delta$ and $-y_s$ with respect to person 1, i.e. person 2 is of the same height or shorter than person 1 (figure 1b). We calculate the flux of aerosols emanating from the mouth of person 1 (ϕ_1) at the ROI located in front of person 2 (who is a susceptible individual) and denote it as
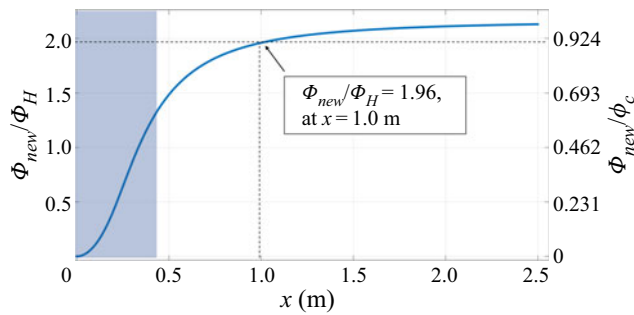
Figure 3. *Comparison of the different characterizations of aerosol concentration. The axial variation of locally averaged aerosol concentration (Φ_{new}) calculated by (3.4) and its comparison with aerosol concentration based on the 'top-hat' formulation (Φ_H). Steady self-similar behaviour is established only for $L_s \gtrsim 0.45$ m.*

$f_{II}(L_s, -y_s/2)$ (3.1a,b). Simulations are performed for three different values of $L_s \in \{0.6, 1.2, 1.8\,\text{m}\}$ with y_s taking one of the seven values among $0d, 2d, 4d, 6d, 8d, 12d$ and $16d$ for each L_s; a couple of other values of y_s are also chosen where needed. As described earlier, each person speaks for 10 speech cycles in a staggered manner to have a total speech time of 70 s (including silent intervals; figure 1d). The simulations are run longer than this duration, until almost all of the aerosols expelled by person 1 pass through the ROI. Figure 4(a) shows the time variation of f_{II} for $L_s = 1.2$ m as y_s is varied, which exhibits a non-monotonic behaviour. As y_s increases from 0, f_{II} increases many folds until $y_s = 8d$ and the time at which f_{II} peaks (at a given y_s) goes on decreasing. As y_s increases beyond $8d$, f_{II} shows a decrease whereas the time at which it peaks increases (figure 4a).

Figure 4(c–e) show the contour plots of the instantaneous aerosol concentration for case II, for $y_s = 0d, 4d, 8d$, respectively, with the colour contours representing different values of ϕ_1 and the line contours representing an isoline for ϕ_1 and ϕ_2 equal to 1.2×10^{-10}; figure 4(b) shows the aerosol contours for case I for comparison. For $y_s = 0d$ (case II; figure 4c), the jets issuing out of the two orifices impinge on each other and 'cancel' out each other's effect to form a cloud in the middle. As a result, the flux of ϕ_1 at person 2 is much smaller for $y_s = 0d$ than it would be if person 2 were silent as in case I (see figure 4b). For $y_s = 4d$, the jets are found to be 'sliding over' each other with a region of overlap in the aerosol distributions (figure 4d). Although the head of flow from person 1 could be seen deviating away from the person 2, the overlapped region of ϕ_1 manages to project a part of the aerosol flux on the latter's face (grey rectangle). For $y_s = 8d$ in figure 4(e), the interference between the two jets is significantly reduced and therefore the aerosols from person 1 find it easier to reach the ROI positioned in front of person 2. For higher y_s, only a small fraction of the speech jet from person 1 can be expected to intersect the ROI, due to the large vertical separation. Thus, the competing effects of the jet interference and vertical separation lead to the observed maximum in the aerosol flux for an intermediate y_s (figure 4a). The blocking effect of the two speech jets for zero vertical separation and the reduced interference between the jets when this separation is increased is also reported by Giri et al. (2022), supporting our observations. The time evolution of the interaction of speech jets from persons 1 and 2 for the cases shown in figure 4(c–e) has been presented as supplementary movie S1 (see supplementary material). The values for $F_{II}(L_s, -0.5 \times y_s, t_c)$ (3.2) are calculated for all the simulations of case II and used to calculate the virion exposure, as explained in next section.

3.3. *Viral exposure and infection probability for cases I and II*

In this section, we determine the virion ingestion by a susceptible individual due to the aerosol transport from speech flows. First, the total virion exposure to a passive listener in case I is calculated using inhaled virions as well as the ones projected onto the eyes and mouth area. The number of inhaled
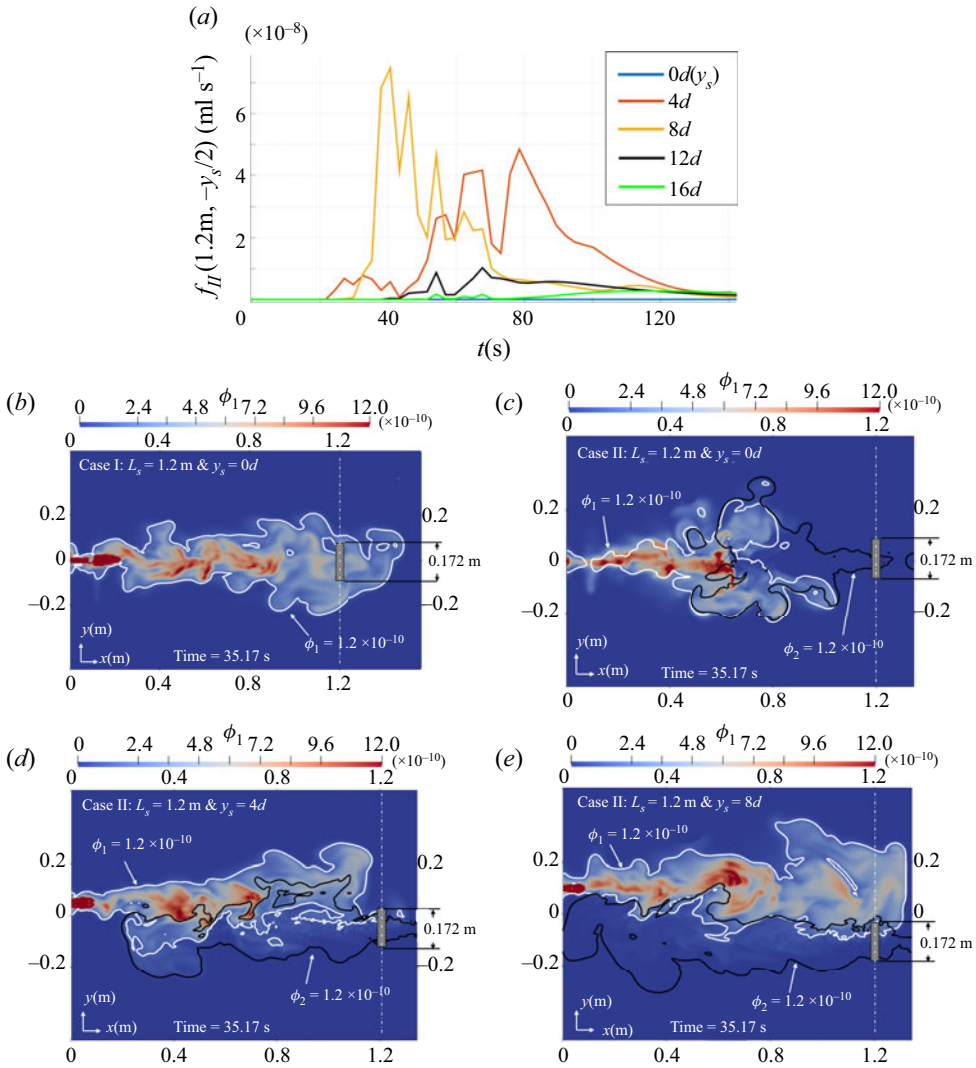
Figure 4. *Aerosol flux distribution and concentration contours for case II (two-way conversation) compared with case I (person 2 silent). (a) Aerosol flux f_{II} for $L_s = 1.2$ m for different vertical separations (y_s) for case II. (b–e) Contours of aerosol concentration for $L_s = 1.2$ m at $t \approx 35$ s for y_s of (b) 0d in case I, (c) 0d in case II, (d) 4d in case II and (e) 8d in case II. In contrast to case I shown in (b), it is evident in (c–e) that the passage of aerosol from one person to another is inhibited by the existence of two speech jets. The outlines of the jets are shown in white for person 1 and black for person 2. Filled colour contours are shown only for ϕ_1. A side view of the circular ROI in front of person 2 is represented by a grey rectangle. Here $\phi_1 = \phi_o (C_{s1}/C_{so})$ and $\phi_2 = \phi_o (C_{s2}/C_{so})$, (see supplementary movie S1 for the time evolution of the interaction between two speech jets for c–e available at https://doi.org/10.1017/flo.2022.7).*

virions in case I is calculated using the same expression as in (3.3) but by replacing Φ_H by Φ_{new} (3.4), as

$$N(\Phi_{new}) = c_v \Phi_{new} Q_r t. \tag{3.5}$$

We use $c_v = 7 \times 10^6$ ml^{-1} (Yang et al., 2020), which is a typical value for the average viral concentration during speech. Note that c_v depends on the loudness of speech, and can be as high as 2×10^9

(Wölfel et al., 2020; Yang et al., 2020); this latter value is used in the exercise presented in §4.2. To calculate the infection through eyes and mouth, we first obtain the total number of virions projected onto the listener's face (or passing through the ROI in front of their face) as $N_{I,f} = c_v F_I(L_s, y_s, 140\,s)$, i.e. integrated over 140 s. Towards this, we use F_I for $y_s = 0$ (blue curve in figure 2b) which corresponds to the maximum aerosol exposure for case I. We assume that viral exposure to the eyes and mouth is the fraction κ of $N_{I,f}$, where $\kappa = A_{em}/A_{ROI}$; here A_{em} is the total area of eyes and mouth, and A_{ROI} is the area of the ROI (i.e. the projected face area). The total number of virions that are ingested by the listener (potentially causing infection) for case I is, therefore,

$$N_{I,i} = N(\Phi_{new}) + \kappa N_{I,f}. \tag{3.6}$$

Reasonable estimates for the areas of the eyes (radius ≈ 1.2 cm) and of the mouth and lips area (≈ 15.55 cm^2), suggest that these amount to approximately 10.6 % of the area of the face ($\kappa = 0.106$).

For case II the total exposure to person 2 over 140 s from the aerosols expelled by person 1 is denoted by $F_{II}(L_s, -0.5 \times y_s, 140\,s)$ ((3.1a,b) and (3.2)). The total virion exposure to the face of person 2 is therefore given as $N_{II,f} = c_v F_{II}(L_s, -0.5 \times y_s, 140\,s)$. To calculate the virion exposure causing infection we assume that

$$N_{II,i}/N_{II,f} = N_{I,i}/N_{I,f}, \tag{3.7}$$

where $N_{II,i}$ represents the number of virions ingested by person 2 through inhalation and exposure to eyes and mouth for a given simulation of case II. Note that $N_{I,i}$ and $N_{II,i}$ represent conservative estimates of ingested virions, assuming that the entire virion exposure to eyes and mouth leads to infection.

Figure 5(a) presents a summary plot of the virion exposure to person 2 (for cases I and II) obtained using different measures. The number of inhaled virions using the method of Yang et al. (2020), $N(\Phi_H)$ (3.3), is plotted as a red dashed curve, whereas $N(\Phi_{new})$ obtained by averaging over a localized region (3.5) is plotted as a black dashed curve. Note that the region $x < 0.45$ m is not considered as self-similarity of speech flow does not hold and calculations using steady state parameters are expected to be unrealistic in this region (figure S15b (supplementary material)). As can be seen from figure 5(a), $N(\Phi_{new})$ is nearly twice that of $N(\Phi_H)$ for the entire range of separation distances, L_s, consistent with figure 3. Note that both $N(\Phi_H)$ and $N(\Phi_{new})$ have been calculated in the context of case I, i.e. with person 2 as a passive listener. The total number of ingested virions for case I, $N_{I,i}$, shows even higher values as compared with $N(\Phi_{new})$ as expected (3.6). We propose that $N_{I,i}$ is a more realistic (although conservative) measure for the viral load for determining the risk of infection, as compared with the estimate based on inhaled virions alone. The number of ingested virions for case II, $N_{II,i}$, is shown as symbols for three different values of L_s. The maximum number of ingested virions for this case at each L_s is seen to occur at an intermediate value of y_s consistent with figure 4(a). Figure 5(a) clearly shows that the viral exposure to person 2 when they are actively engaged in a conversation (case II) is lower as compared with that when person 2 is a passive listener (case I) by a factor more than two. This is due to the interference of the speech jets from the two persons during a conversation as discussed earlier.

In figure 5(b) we plot the probability of infection corresponding to the viral load N calculated as

$$p(N) = 1 - \exp(-N/N_{inf}), \tag{3.8}$$

where $N_{inf} \approx 100$ is the characteristic number of virions causing infection (Yang et al., 2020). For case I, $p(N_{I,i})$ is found to be as high as 0.5 when $L_s = 0.6$ m. Thus, there is a real risk of inflection to a passive listener for a 0.6 m separation distance, even when the other person speaks for a very short time (speech time = 70 s and exposure time = 140 s). As the separation distance increases the infection probability decreases monotonically, with $p(N_{I,i}) < 0.2$ for $L_s = 1.8$ m (figure 5b). Thus, it is much safer to adhere to the 6 ft (approximately 1.8 m) rule even while listening to someone speak for a short span of time, in order to minimize the risk of infection. For case II involving conversations, $p(N_{II,i})$ is much less than $p(N_{I,i})$ as expected and the risk of infection is therefore low. The maximum $p(N_{II,i})$ among all the
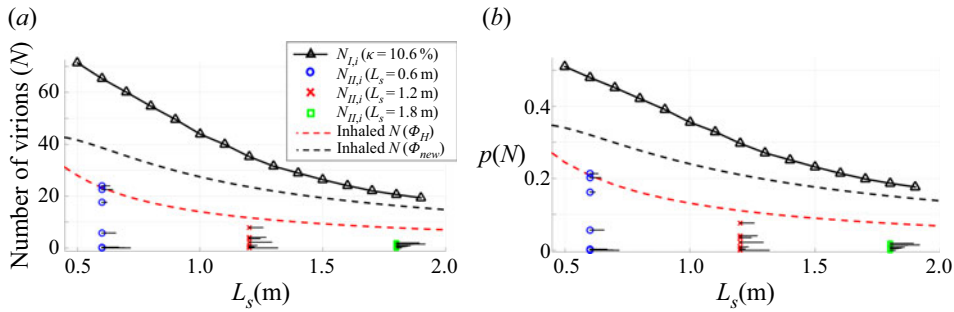
Figure 5. *(a) The number of virions and (b) the probability of infection for case I (curves) and case II (symbols). Each symbol for case II corresponds to a different simulation. The probability of infection in case II is always much lower than in case I, which means that a dialogue is always better than a monologue. The red-dashed curve, showing viral exposure through inhalation alone, calculated using the method by* Yang et al. (2020), *is always lower by approximately 50 % than the solid black curve which includes exposure to the eyes and the mouth. The locations of the symbols correspond to the axial separation L_s between the speakers and each symbol is accompanied by a horizontal bar whose length is proportional to y_s, for $y_s \in \{0d, 2d, 4d, 6d, 8d, 12d, 16d\}$. In case II, the infection probability for a given L_s varies non-monotonically with y_s.*
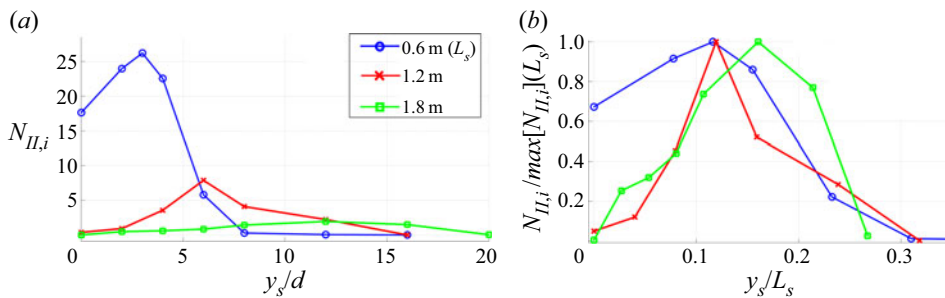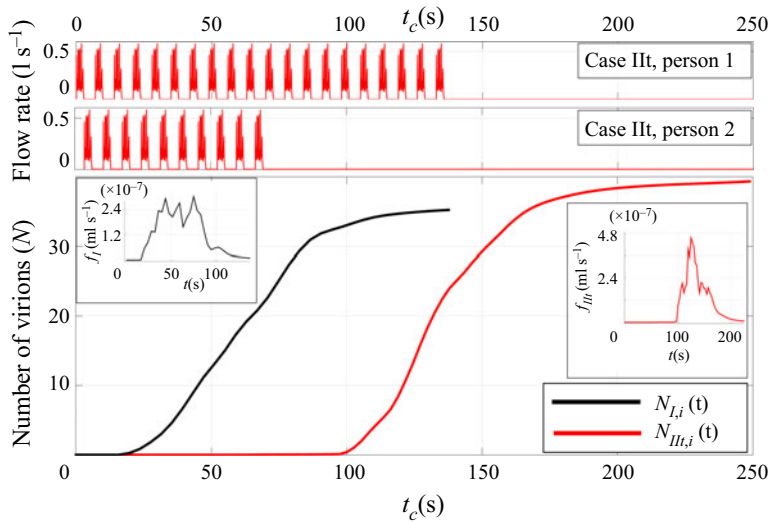

Figure 6. *(a) The number of virions $N_{II,i}$ ingested by person 2 as a function of the vertical separation y_s/d for different axial separations L_s. (b) Variation of normalized $N_{II,i}$ with y_s/L_s. Risk of infection varies non-monotonically with vertical separation.*

conversation cases is approximately 0.2 for $L_s = 0.6$ m for a conversation of a little over a minute. For a longer conversation or for asymmetric speech times (see the next section) between the people, the risk of infection can be expected to be higher than this. Increasing separation between people during conversation is again a certain way of reducing the infection probability (figure 5b).

Figure 6(a) provides a graphical representation of the dependence of $N_{II,i}$ on L_s and y_s. As follows from the discussion above, the viral dose to person 2 decreases considerably with increase in L_s and $N_{II,i}$ peaks at an intermediate vertical separation y_s (see also figure 5). Figure 6(b) plots the variation of the normalized viral dose (by its peak value for a given L_s) with y_s/L_s. We find that maximum of the normalized $N_{II,i}$ occurs at y_s/L_s of 0.12–0.15 which can be a useful result from the scaling point of view. Furthermore, $N_{II,i}/max(N_{II,i})$ is significantly reduced for $y_s/L_s > 0.3$, implying that for a given separation distance between two people, the viral load during a short conversation can be expected to be low if the condition $y_s \gtrsim L_s/3$ is satisfied.

Giri et al. (2022) found the 'critical' vertical separation for a maximum exposure to infected aerosols during a conversation to be $2y_s/(L_s \tan(\alpha)) \approx 0.83$ (where α is the jet half-angle), which translates into $y_s/L_s \approx 0.087$, using $\alpha = 11.8°$ (Giri et al., 2022). They did this exercise for $L_s = 1$ m. This value is

Figure 7. *The role of temporal asymmetry in determining viral exposure, shown by plotting (bottom subpanel) the number of virions ingested as a function of time in case IIt compared with case I. The subpanels at the top show the inlet flow rates. For both cases $L_s = 1.2$ m and $y_s = 0$. For case IIt, the conversation does not stop incoming aerosols from reaching person 2 but merely delays it by approximately 100 s (see supplementary movie S2 for time evolution of the flow for this case). The time variation of $N_{IIt,i}$ shown here can in principle be extrapolated to estimate the viral load for conversations longer than used here.*

somewhat smaller than the $y_s/L_s \approx 0.12$ that we obtained for maximum aerosol exposure to person 2 for $L_s = 1.2$ m (figure 6b). The difference between the two studies can be attributed to two factors. First, Giri et al. (2022) use a different parameter than we do to determine the critical vertical separation – they base it on the fraction of the total number of particles released by the speaker that reaches the 'zone of influence' of the listener. Second, the speech duration used for their exercise is short, approximately 25–30 s. In contrast, we determine the critical separation using the estimates of ingested virions (3.6) and (3.7) over an extended period of 140 s.

3.4. Case IIt: temporal asymmetry in speech during conversation

So far, we have presented conversation cases where the number of speech cycles and the total speech time were the same for persons 1 and 2 (figure 1d). This corresponds to a scenario wherein the exchange of short phrases during a conversation is more or less 'symmetric' (although staggered in time). The objective of this exercise was to quantify the difference between one-way and two-way conversations. However, in reality, conversations can take place in a variety of different ways and in most of the cases there is likely to be an asymmetry of speech between two people. Here we present one instance of an 'asymmetric' conversation (case IIt) wherein both the persons engage in a symmetric conversation for 70 s, after which person 2 stops talking while person 1 continues for another 70 s; see figure 7. Both the persons are considered to be of equal height ($y_s = 0$) with a separation distance, $L_s = 1.2$ m, and the simulation is run for approximately 250 s. Figure 7 shows the variation of the number of virions ingested, $N_{IIt,i}$, with time interval, t_c, obtained by varying t_c in the calculation of $F(L_s, y_s, t_c)$ in (3.2) for case IIt. Also shown for comparison is $N_{I,i}(t_c)$ for case I representing a one-way conversation. It is seen that the number of ingested virions for case IIt is negligibly small until approximately 100 s (cf. figure 4a) after which $N_{IIt,i}$ starts increasing as the aerosols from person 1 (who continues to speak after 70 s) reach person 2. The increase in $N_{IIt,i}$ is initially rapid but tapers off after person 1 stops
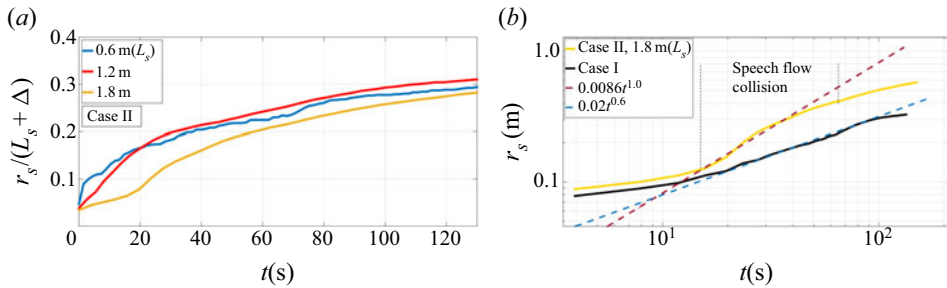
Figure 8. *(a) Lateral width (r_s from (4.1)) normalized by the corresponding domain length between the two persons for case II. (b) Lateral width of the flow on a log–log scale for cases I and II, with $L_s = 1.8$ m. For case II, $y_s = 0$.*

speaking after 140 s. Overall, the shapes of curves and the number of virions ingested by person 2 at the end of conversation are similar between $N_{IIt,i}$ and $N_{I,i}$ (figure 7).

The probability of infection for person 2 at $t_c = 250$ s for case IIt comes out to be $p(N_{IIt,i}) = 0.32$ (3.8), which is slightly higher than that obtained for case I (figure 5b). This suggests that whenever there is an asymmetry in speech between people engaged in a conversation, the person who talks less is at an enhanced risk of catching an infection than the person who talks more. This is true even when both the persons are of nearly the same height. The time evolution of the speech jets for case IIt is presented as supplementary movie S2 (see supplementary material). Note that the asymmetry in time need not occur at the end of a conversation but could be embedded within it, in which case the curve for $N_{IIt,i}$ in figure 7 will show an 'up and down' variation, providing temporally varying and non-monotonic probability of infection.

4. Discussion

4.1. Lateral spread and temporal evolution of the interacting speech jets

Although the collision of the speech jets during conversations can restrict the axial transport of aerosols (especially for people of comparable heights; figure 4), it can result in considerable lateral spread of the flow. This aspect is relevant to how the interaction of two people generates a 'cloud' of infected aerosols that might affect disease spread in poorly ventilated rooms. We define the lateral width (r_s) of the flow using

$$\int_{r=0}^{r_s} \int_\theta \int_x \phi r \, dr \, d\theta \, dx = 0.9 \int_{r=0}^{\infty} \int_\theta \int_x \phi r \, dr \, d\theta dx. \qquad (4.1)$$

The lateral widths of the flow in case II (two-speaker) simulations are compared for different axial separations in figure 8(a), and with case I (single-speaker case) in figure 8(b). The axial length of the domain, $L_s + \Delta$ ($\equiv L_x$; see figure 1b), acts as a rough scaling length for the lateral spread (figure 8a); $r_s/(L_s + \Delta)$ reaches a value of 0.3 after 120 s, which is approximately 0.55 m for $L_s = 1.8$ m. Figure 8(b) shows that the collision of the speech jets from the two persons initially increases the rate of lateral spread ($r_s \propto t^{1.0}$), which is significantly higher than that in case I where lateral spread is $\propto t^{0.6}$. This provides an estimate of the rate of evolution of the aerosol cloud that might affect a third person positioned nearby; it should also be possible to extrapolate the rate of growth for longer conversation times using the power laws in figure 8(b). At later times, i.e. after the conversation ends, the rate of spread in case II becomes slower, but the lateral spread continues to remain much larger than that for case I.

In figure 9(a), we plot the location of the stagnation point, x_s, between the two speech jets for case II. For small axial separation as $L_s = 0.6$ m, we see that the location of the stagnation point nearly reaches either speaker at $(2x_s/(L_s + \Delta)) - 1 = \pm 1$. This wide oscillation is responsible for the non-zero aerosol
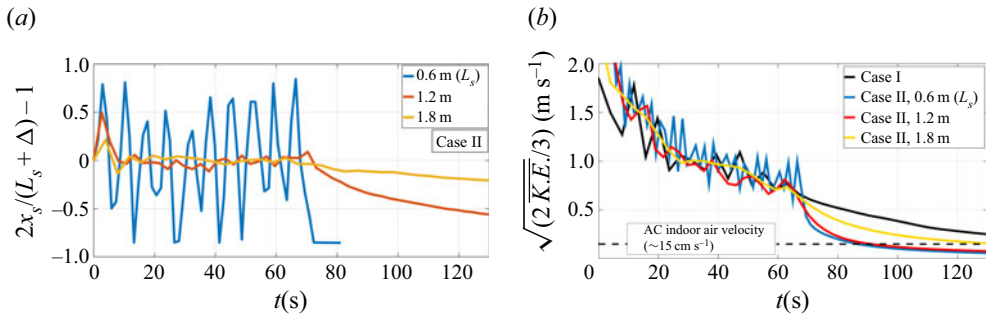
Figure 9. *(a) Flow oscillation due to the collision of alternate speech jets from two people, represented by the stagnation point (x_s) in the centreline velocity distribution. The location x_s is normalized such that person 1 is at $x = -1$ and person 2 is at $x = 1$. See supplementary movie S3 for time variation of the stagnation point for $L_s = 0.6$ m. (b) A measure of average velocity, based on the domain-averaged kinetic energy, as a function of time for cases I and II. For case II, $y_s = 0$. The dashed line indicates the velocity for a typical air current in an air-conditioned (AC) room.*

flux even in a face-to-face ($y_s = 0$) conversation for $L_s = 0.6$ m (see figure 6). This is not true, however, for larger axial separations L_s. The oscillation of the stagnation point is a feature of the pulsatile nature of the flow and is not captured if the flows are taken to be steady jets (for which the stagnation point would remain fixed in place at mid-domain). The oscillation of the stagnation point also suggests that the 'safe' axial separation between two persons facing each other depends on the duration of the speech pulses in figure 9(*a*). Following Abkarian et al. (2020), the time (t^*) taken by a jet to reach the separation distance L_s scales as $t^* \approx L_s^2 \tan \alpha / 2\bar{v}_o d$, which gives $t^* \approx (3.34, 13.35$ and 30.04 s) for $L_s = (0.6, 1.2$ and 1.8 m), respectively. For $L_s = 0.6$ m, the estimate $t^* \approx 3.34$ s is comparable to the half of the speech-cycle duration, which is 3.5 s. Note that the average orifice velocity $\bar{v}_o = 0.39$ m s^{-1}.

Figure 9(*b*), plots the time variation of a measure of velocity related to the averaged kinetic energy as $\sqrt{2\overline{K.E.}}/3$, with $\overline{K.E.}$ defined as follows:

$$\overline{K.E.} = \frac{1/2 \int (u^2 + v^2 + w^2)\, dV \Big|_{\phi > 0.01\phi_o}}{\int dV \Big|_{\phi > 0.01\phi_o}}, \tag{4.2}$$

where V represents the domain volume. The decay of the domain-averaged kinetic energy is nearly identical for cases I and II until the end of the speech duration (i.e. 70 s), after which the kinetic energy decays at different rates for different cases. The decay rate is larger for the two lower values of L_s (case II), presumably because of the enhanced dissipation resulting from more intense gradients generated by the collision of speech jets; figure 9(*b*). The residual velocity in the domain reaches fairly low values after the conversation ends and can soon become comparable to the speed of the background air motion found in typical indoor environments. For example, a threshold background current in an air-conditioned room is of the order of 15 cm s^{-1} (Matthews, Thompson, Wilson, Hawthorne, & Mage, 1989), shown by dashed horizontal line in figure 9(*b*). Under such conditions, the transport of virus-laden aerosols can be expected to switch to the airborne transmission mode.

4.2. Factors influencing the risk of infection

From (3.3), (3.5) and (3.8), we see that the kernel used in calculating the probability of infection, N/N_{inf}, is proportional to $c_v \phi_o/N_{inf}$, to be denoted as χ (with the average inhalation rate Q_r taken as

Table 1. *Dependence of probability of infection on the numerical values of number of virions per droplet volume (c_v), liquid volume fraction at the orifice (ϕ_o) and minimum dose of virions for infection N_{inf}.*

Parameters	c_v (ml^{-1})	ϕ_o	N_{inf}	$\chi = c_v \phi_o / N_{inf}$	$p(N_{II,i})$ ($L_s = 1.2$ m, $y_s = 6d$)
Set 1	7.0×10^6	6.0×10^{-9}	100	4.2×10^{-4}	7.6 %
Set 2	2.0×10^9	1.0×10^{-8}	100	2.0×10^{-1}	≈ 100 %
Set 3	2.0×10^9	1.0×10^{-8}	5.0×10^5	4.0×10^{-5}	0.75 %

constant $= 0.11$ s^{-1}). Thus the viral dose and the probability of infection depend on the precise values prescribed for each of these parameters. The values used in the present analysis, which are representative of 'typical' speech (§ 3), are listed in table 1 and denoted as 'set 1'. As noted in § 3, for 'loud' speech, the values of c_v and ϕ_o can be much larger and these are included in table 1 as 'set 2'. We do not study the effect of loudness of speech on the flow velocities at the orifice, consistent with Giri et al. (2022) and Yang et al. (2020). The minimum dose of virions needed for infection that we have prescribed is $N_{inf} = 100$ and the same number is used for set 2. Note that there is still a lack of consensus on the minimum viral dose of SARS-CoV-2 needed for a susceptible individual to contract COVID-19 infection. The minimum viral load required for disease transmission also depends on the particular strain of the virus (the 'omicron' strain is much more transmissible, for instance). A recent study by Poydenot et al. (2021) estimates N_{inf} to be as high as 5×10^5, and we have included this value in 'set 3', with c_v and ϕ_o same as those in set 2. Incidentally, the parameters in set 3 are the same as used by Giri et al. (2022) for estimating the probability of infection when the speaker is a 'super-titerer' (i.e. a person who has very high viral load in their saliva). As can be seen from table 1, χ is three orders of magnitude larger for set 2 as compared with set 1, and is one order of magnitude smaller for set 3 compared with set 1. This can result in a considerable variation in the estimates of infection risk. As an example, we have calculated the probability of infection ($p(N_{II,i})$) for one of our conversation cases (case II) with $L_s = 1.2$ m and $y_s = 6d$; see table 1. For set 1, $p(N_{II,i}) = 7.6$ % as calculated earlier (figure 5b). For set 2, the probability increases to nearly 100 %, representing a possible 'superspreading' instance. For set 3, $p(N_{II,i}) = 0.75$ %, which is negligibly small due to the very large value of N_{inf} used. Note that the qualitative conclusions drawn from the present results are not affected by this variation, as the viral dose changes by the same factor, for any combination of L_s and y_s, when the parameter values in table 1 are changed.

Thus, an accurate specification of the values of viral parameters such as c_v, ϕ_o and N_{inf} (among others) is crucial for an accurate estimation of the risk of infection. The probabilities of infection for two combinations of parameters may be related to each other, combining equations (3.3), (3.5) and (3.8), using

$$p_2(N) = 1 - \exp\left[\frac{\chi_2}{\chi_1} \ln(1 - p_1(N))\right], \tag{4.3}$$

where the subscripts 1 and 2 refer to the two parameter sets under consideration. Equation (4.3) can, in principle, be used to update the risk of infection as new strains of the SARS-CoV-2 arise, with their own sets of values for the parameters in table 1.

The other factors that influence the risk of infection are the duration of speech as discussed in § 3.3 and the measure of total viral exposure used in calculating the probability of infection. For example, the method used by Giri et al. (2022), which is essentially the same as that proposed by Yang et al. (2020), considers only the inhaled virions and therefore results in probabilities lower than our estimates, which also include viral exposure to eyes and mouth. Furthermore, the results presented here are relevant for poorly ventilated spaces whereas a cross-ventilation can make a difference in the number of ingested virions. Finally, the speech cycles used are based on utterance of simple repetitive phrases and therefore can only serve as an approximation to the real speech patterns. Notwithstanding these uncertainties,
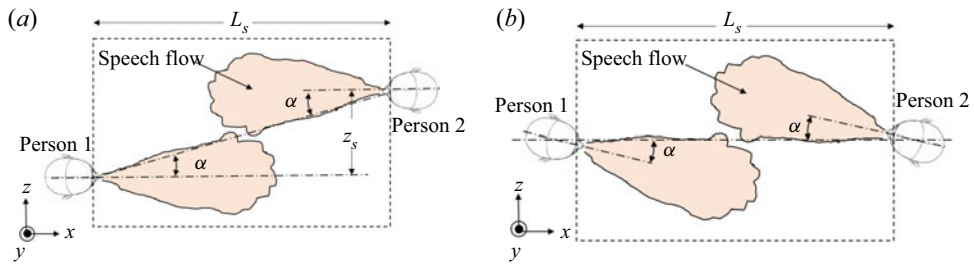
Figure 10. *Lateral/angular separation to minimize transmission risk. (a) Schematic of two persons separated laterally by a distance z_s such that the risk of infection is minimized. (b) Schematic of two people conversing with their heads turned away from each other by an 'angular separation' to achieve the same effect as in (a). For an axial separation up to 1.8 m, a tilt angle (α) of 9° or more is recommended.*

our simulations provide general scientific principles on which public health guidelines can be based, as discussed below.

4.3. Relevance towards public health guidelines and epidemiological modelling

Our results provide guidance, in addition to physical distancing, for safe interaction among people engaged in short conversations (up to approximately a minute or two). This situation arises routinely in day-to-day life, for example in shopping centres, where over-the-counter conversations take place for short durations. We show the effect of buoyancy to be negligible, since the rate of spread of the speech flow in the vertical and horizontal planes is practically identical (see figure S13 (supplementary material)). So our results on the height difference (vertical separation y_s) between two people also apply to lateral separation (denoted by z_s; figure 10). This is an important result since it is easier to control the lateral separation between people than the vertical separation. We find that the probability of infection from a two-way conversation is maximum, not when the two people face each other directly, but when y_s (or z_s) is approximately 12 %–15 % of L_s (figure 6b); for an axial separation of 1.2 m, this amounts to approximately 15 cm of vertical or lateral separation. However, infection probability is considerably lower when y_s/L_s (or z_s/L_s) is greater than 0.3 (figure 6b) and this helps in devising the following general rule for minimizing the risk of infection. When people in a conversation turn their faces away from each other very slightly, it can be worse than facing each other directly, but an angle greater than $\tan^{-1}(0.18/1.2) \approx 9°$ (figure 10b) can be very helpful. This implies a total 'angular separation' of 18° or more between two people for a safe conversation which still enables eye contact. This angular separation matches well with the angle of spread of the speech jet ($\approx 20°$; figure S13 (supplementary material)), which means that the speech jet from one person effectively misses the face of the other person, thereby minimizing viral exposure. As expected, for the three axial separations considered, the probability of infection is the least for $L_s = 1.8$ m (figure 5).

Note that the above results are based on the 'directed jet' behaviour of speech flow (which is the main cause of the sustained aerosol transport away from the speaker's mouth) generated by the repetition of the phrase 'Peter Piper picked a peck' (Abkarian et al., 2020). Abkarian et al. (2020) also considered other phrases containing fricatives and plosives, and found that the flow associated with the utterance of isolated syllables could be directed upward or downward from the axis at angles as high as 40°–50°. However, these flow patterns are contained within a distance of 0.5 m from the speaker and die out within 100 ms after they are expelled from the mouth (Abkarian et al., 2020). For two people separated by more than 0.6 m and for time scales of interaction of the order of one to two minutes as considered here, the transient aerosol transport associated with individual syllables is likely to be less relevant. It will of course be better if the listener can stay entirely outside the zone of influence of the speech flow as suggested by Abkarian et al. (2020), although it may not be always possible.

Based on our simulations (and taking cues from previous studies), we formulate the following guidelines for short unmasked conversations.

 (i) A two-way conversation is far better than a monologue, so it is better to avoid extended one-way conversations. The person who talks less is at a higher risk of infection.
 (ii) In close-up conversations, a slight tilt of the head or a small lateral separation, even while maintaining eye contact, can help in minimizing risk of infection.
(iii) As expected, the greater the separation between two people the better, not only while coughing/ sneezing but even during conversations.

Note that the above guidelines are based on idealized simulation conditions and do not include effects of indoor ventilation, outdoor winds, natural convection flow due to human-body surface temperature, etc. However, they can provide useful pointers for devising more general public-health measures. Moreover, in view of the large number of variables involved in estimating the infection risk as discussed in § 4.2, and the inherent complexity of speech flows, we believe mask mandates continue to be crucial in curbing disease transmission (Bagheri, Thiede, Hejazi, Schlenczek, & Bodenschatz, 2021; Chu et al., 2020).

The present results can also provide useful inputs to epidemiological models to improve their prediction accuracy. In this connection, Chaudhuri et al. (2020) have presented a framework for determining the infection rates for different expiratory events such as coughing, sneezing, breathing, talking, etc. and incorporating them in an SEIRD (susceptible–exposed–infected–recovered–deceased) model (see also Dbouk and Drikakis (2021)). They have highlighted the need for accurate data on viral exposure based on fluid dynamical simulation of these expiratory events. Since the present simulations provide a spatiotemporal distribution of the aerosol field for speech flows, the quantities of interest can be easily calculated, e.g. the temporal variation of the viral load presented in figure 7 can be used for determining time-dependent infection probabilities for speech flows, which is a crucial input to the model used in Chaudhuri et al. (2020). For realistic conversation scenarios these probabilities could not have been accurately inferred from the idealized cases of 'one-way' conversation (which would overestimate the risk) or 'symmetric' conversation (which would underestimate the risk).

5. Summary of key results

We have performed DNS of the turbulent transport of aerosols by the flows generated in human speech (involving repetitive utterance of certain phrases) during short conversations. The speech cycle consists of a certain duration of speaking a phrase (exhalation) followed by a period of silence; we do not include inhalation as it has a negligible effect on the overall flow field and the aerosol transport towards the listener. The Boussinesq–Navier–Stokes equations are solved without including the thermodynamic effects of evaporation. This is justified as the very small speech droplets evaporate quickly turning into droplet nuclei (with negligible change in flow buoyancy), which can be modelled as passive scalars. The main results from our work are the following.

1. We have computed the total exposure to aerosol on a listener due to speech flow from a speaker not only through inhalation but also through the mouth and eyes. A conservative estimate of the probability of infection is calculated based on the total number of ingested virions and is shown to be higher by a factor of 2 or more compared with previous estimates.
2. In conversations, the active involvement of both people significantly lowers the aerosol exposure (and the associated risk of infection) with respect to the case where one person is a passive listener. This is because of the interference between the two speech jets, which effectively shuts off onward transmission of infected aerosols. On the other hand, asymmetry in the speech pattern of two people, invariably present in real conversations, reduces the jet interference and enhances the risk of infection to the person who talks less.
3. For identical speech phrases from both speakers, the probability of infection peaks when there is a small vertical/lateral separation between them, due to a less effective interaction between the two

jets. When this separation is greater than 0.3 times the axial (perpendicular) distance between them, the risk of infection is seen to be minimal.

4. The collision of the speech jets results in a considerable lateral spread of the aerosol cloud potentially infecting surrounding air in an indoor environment. For small axial separations between two people, the speech jets oscillate considerably in time and can penetrate to reach the other person's face in an intermittent fashion.

5. The probability of infection is shown to sensitively depend on the parameters relevant for viral transmission, highlighting the need for a more accurate determination of such parameters specific to SARS-CoV-2 and its variants.

The observation that a small vertical separation between two conversing people can enhance the aerosol exposure on either of them was also reported in a concurrent paper by Giri et al. (2022), which appeared while the present paper was under revision. The analysis presented here is more comprehensive and we have obtained several new results on the risk of infection for a wide variety of speech scenarios as listed above. We believe simulations such as the ones presented here can provide realistic estimates of infection probabilities for any speech pattern of interest and can provide useful inputs to epidemiological models. Moreover, our results provide insights into the complexity of deciding foolproof public health guidelines to curb the spread of COVID-19.

Appendix A. Governing equations and numerical method

The Boussinesq–Navier–Stokes equations, with scalar transport equations for temperature and passive scalar, are given as

$$\tilde{\boldsymbol{\nabla}} \cdot \tilde{\boldsymbol{u}} = 0, \tag{A1}$$

$$\mathrm{D}\tilde{\boldsymbol{u}}/\mathrm{D}\tilde{t} = -\tilde{\boldsymbol{\nabla}}\tilde{p} + \frac{1}{Re}\tilde{\nabla}^2\tilde{\boldsymbol{u}} + \frac{1}{Fr^2}\tilde{\theta} e_y, \tag{A2}$$

$$\mathrm{D}\tilde{\theta}/\mathrm{D}\tilde{t} = \frac{1}{Re\,Pr}\tilde{\nabla}^2\tilde{\theta}, \tag{A3}$$

$$\mathrm{D}\tilde{C}_s/\mathrm{D}\tilde{t} = \frac{1}{Re\,Sc}\tilde{\nabla}^2\tilde{C}_s, \tag{A4}$$

where $\tilde{u}$ is the fluid velocity, $\tilde{p}$ is the pressure, $\tilde{\theta}$ is the temperature difference between the flow and the ambient, $\tilde{C}_s$ is the passive scalar concentration, $\mathrm{D}/\mathrm{D}t$ is the material derivative, $Re = u_c d/\nu$ is the Reynolds number, $Fr^2 = u_c^2/\beta dg\Delta T_o$ is the Froude number squared, ν is kinematic viscosity of air, g is acceleration due to gravity, β is the coefficient of thermal expansion for air and non-dimensional quantities are represented by a tilde ˜. The density difference between the speech fluid and the ambient is given by $\Delta\rho/\rho = -\beta\Delta T$; with $\beta \approx 3.4 \times 10^{-3}\,\mathrm{K}^{-1}$ and a temperature difference at the orifice,

$\Delta T_o = 14\,^\circ$C, we get $\Delta\rho/\rho \approx -0.05$, supporting the Boussinesq approximation. The passive scalar at the orifice is taken as unity, $C_{so} = 1$. The governing parameters are the Prandtl number, Pr, and the Schmidt number Sc governing the diffusion of the temperature and scalar, respectively, which are both assigned unit values. For the length and velocity scales mentioned above characteristic of respiratory flows, $Re = 1906$ and $Fr^{-2} = 0.00842$. For the conversation cases (with both the persons speaking) two equations are solved for the passive scalar – one each for $\tilde{C}_{s1}$ and $\tilde{C}_{s2}$.

The DNS solver Megha-5 which has been used previously for canonical jets, plumes (Singhal et al., 2021) and cumulus and mammatus clouds (Ravichandran, Meiburg, & Govindarajan, 2020; Ravichandran & Narasimha, 2020), is employed here. The governing equations are discretized on a staggered Cartesian (Arakawa-C) mesh, with velocities stored on cell-faces and scalar quantities (including the pressure) saved at cell-centres (see Patankar (2018); chapter 6). The advection terms in both the momentum and the scalar equations are calculated using a second-order conservative discretization, and the viscous terms are treated explicitly. We use the operator-splitting technique of Chorin (1968) to update the velocities and a cosine-transform-based Poisson solver (similar to the AFiD solver; (Van Der Poel, Ostilla-Mónico, Donners, & Verzicco, 2015) to compute the pressure correction. A second-order accurate Adams–Bashforth scheme is used for time advancement with time steps decided based on a Courant–Friedrichs–Lewy number of 0.15. For more details, see Singhal et al. (2021) and Ravichandran et al. (2020).

References

Abkarian, M., Mendez, S., Xue, N., Yang, F., & Stone, H.A. (2020). Speech can produce jet-like transport relevant to asymptomatic spreading of virus. *Proceedings of the National Academy of Sciences of the United States of America*, *117*(41), 25237–25245. https://doi.org/10.1073/pnas.2012156117

Asadi, S., Bouvier, N., Wexler, A.S., & Ristenpart, W.D. (2020a). The coronavirus pandemic and aerosols: Does COVID-19 transmit via expiratory particles? *Aerosol Science and Technology*, *54*(6), 635–638. https://doi.org/10.1080/02786826.2020.1749229

Asadi, S., Wexler, A.S., Cappa, C.D., Barreda, S., Bouvier, N.M., & Ristenpart, W.D. (2020b). Effect of voicing and articulation manner on aerosol particle emission during human speech. *PloS One*, *15*(1), e0227699.

Asadi, S., Wexler, A.S., Cappa, C.D., Barreda, S., Bouvier, N.M., & Ristenpart, W.D. (2019). Aerosol emission and superemission during human speech increase with voice loudness. *Scientific Reports*, *9*(1), 1–10. https://doi.org/10.1038/s41598-019-38808-z

Bagheri, G., Thiede, B., Hejazi, B., Schlenczek, O., & Bodenschatz, E. (2021). An upper bound on one-to-one exposure to infectious human respiratory particles. *Proceedings of the National Academy of Sciences*, *118*(49), e2110117118.

Balachandar, S., Zaleski, S., Soldati, A., Ahmadi, G., & Bourouiba, L. (2020). Host-to-host airborne transmission as a multiphase flow problem for science-based social distance guidelines. *International Journal of Multiphase Flow,132*, 103439.

Basu, S. (2021). Computational characterization of inhaled droplet transport to the nasopharynx. *Scientific Reports*, *6652*. https://doi.org/10.1038/s41598-021-85765-7

Basu, S., Kabi, P., Chaudhuri, S., & Saha, A. (2020). Insights on drying and precipitation dynamics of respiratory droplets from the perspective of COVID-19. *Physics of Fluids*, *32*(12), 123317. https://doi.org/10.1063/5.0037360

Bhardwaj, R., & Agrawal, A. (2020). Likelihood of survival of coronavirus in a respiratory droplet deposited on a solid surface. *Physics of Fluids*, *32*(6), 061704. https://doi.org/10.1063/5.0012009

Bourouiba, L. (2020). Turbulent gas clouds and respiratory pathogen emissions: Potential implications for reducing transmission of COVID-19. *JAMA - Journal of the American Medical Association*, *323*(18), 1837–1838. https://doi.org/10.1001/jama.2020.4756

Bourouiba, L. (2021). The fluid dynamics of disease transmission. *Annual Review of Fluid Mechanics*, *53*, 473–508. https://doi.org/10.1146/annurev-fluid-060220-113712

Bourouiba, L., Dehandschoewercker, E., & Bush, J.W.M. (2014). Violent expiratory events: On coughing and sneezing. *Journal of Fluid Mechanics*, *745*, 537–563. https://doi.org/10.1017/jfm.2014.88

Chaudhuri, S., Basu, S., & Saha, A. (2020). Analyzing the dominant SARS-CoV-2 transmission routes toward an ab initio disease spread model. *Physics of Fluids*, *32*(12), 123306. https://doi.org/10.1063/5.0034032

Chen, X., Yu, H., Mei, T., Chen, B., Chen, L., Li, S., Zhang, X., & Sun, X. (2020). SARS-CoV-2 on the ocular surface: Is it truly a novel transmission route? *British Journal of Ophthalmology*, *105*(9), 1190–1195. https://doi.org/10.1136/bjophthalmol-2020-316263

Chong, K.L., Ng, C.S., Hori, N., Yang, R., Verzicco, R., & Lohse, D. (2021). Extended lifetime of respiratory droplets in a turbulent vapor puff and its implications on airborne disease transmission. *Physical Review Letters*, *126*(3), 34502. https://doi.org/10.1103/PhysRevLett.126.034502

Chorin, A.J. (1968). Numerical solution of the Navier–Stokes equations. *Mathematics of Computation*, *22*(104), 745–762.

Chu, D.K., Akl, E.A., Duda, S., Solo, K., Yaacoub, S., Schünemann, H.J., . . . Reinap, M. (2020). Physical distancing, face masks, and eye protection to prevent person-to-person transmission of SARS-CoV-2 and COVID-19: A systematic review and meta-analysis. *The Lancet*, *395*(10242), 1973–1987. https://doi.org/10.1016/S0140-6736(20)31142-9

Clark, R.P., & De Calcina-Goff, M.L. (2009). Some aspects of the airborne transmission of infection. *Journal of the Royal Society Interface*, *6*(Suppl. 6), S767–S782. https://doi.org/10.1098/rsif.2009.0236.focus

Coroneo, M.T., & Collignon, P.J. (2021). Comment SARS-CoV-2: Eye protection might be the missing key. *The Lancet Microbe*, *5247*(21), 19–20. https://doi.org/10.1016/S2666-5247(21)00040-9

Dbouk, T., & Drikakis, D. (2020). On coughing and airborne droplet transmission to humans. *Physics of Fluids*, *32*(5), 53310.

Dbouk, T., & Drikakis, D. (2021). Fluid dynamics and epidemiology: Seasonality and transmission dynamics. *Physics of Fluids*, *33*(2), 21901.

Duguid, J.P. (1946). The size and the duration of air-carriage of respiratory droplets and droplet-nuclei. *Journal of Hygiene*, *44*(6), 471–479. https://doi.org/10.1017/S0022172400019288

Fabregat, A., Gisbert, F., Vernet, A., Dutta, S., Mittal, K., & Pallarès, J. (2021). Direct numerical simulation of the turbulent flow generated during a violent expiratory event. *Physics of Fluids*, *33*(3), 35122.

Giovanni, A., Radulesco, T., Bouchet, G., Mattei, A., Révis, J., Bogdanski, E., & Michel, J. (2021). Transmission of droplet-conveyed infectious agents such as SARS-CoV-2 by speech and vocal exercises during speech therapy: Preliminary experiment concerning airflow velocity. *European Archives of Oto-Rhino-Laryngology*, *278*, 1687–1692. https://doi.org/10.1007/s00405-020-06200-7

Giri, A., Biswas, N., Chase, D.L., Xue, N., Abkarian, M., Mendez, S., . . . Stone, H.A. (2022). Colliding respiratory jets as a mechanism of air exchange and pathogen transport during conversations. *Journal of Fluid Mechanics*, *930*, R1.

Greenhalgh, T., Jimenez, J.L., Prather, K.A., Tufekci, Z., Fisman, D., & Schooley, R. (2021). Ten scientific reasons in support of airborne transmission of SARS-CoV-2. *Lancet*, *6736*(21), 2–4. https://doi.org/10.1016/S0140-6736(21)00869-2

Gregson, F.K.A., Watson, N.A., Orton, C.M., Haddrell, A.E., McCarthy, L.P., Finnie, T.J.R., . . . Reid, J.P. (2021). Comparing aerosol concentrations and particle size distributions generated by singing, speaking and breathing. *Aerosol Science and Technology*, *55*(6), 681–691.

Gupta, J.K., Lin, C.-H., & Chen, Q. (2009). Flow dynamics and characterization of a cough. *Indoor Air*, *19*(6), 517–525.

Haselton, F.R., & Sperandio, P.G.N. (1988). Convective exchange between the nose and the atmosphere. *Journal of Applied Physiology*, *64*(6), 2575–2581. https://doi.org/10.1152/jappl.1988.64.6.2575

Johnson, G.R., Morawska, L., Ristovski, Z.D., Hargreaves, M., Mengersen, K., Chao, C.Y.H., . . . Corbett, S. (2011). Modality of human expired aerosol size distributions. *Journal of Aerosol Science*, *42*(12), 839–851. https://doi.org/10.1016/j.jaerosci.2011.07.009

Kolinski, J.M., & Schneider, T.M. (2020). Superspreading events suggest aerosol transmission of SARS-CoV-2 by accumulation in enclosed spaces. *Physical Review E, 103*, 033109.

Liu, K., Allahyari, M., Salinas, J.S., Zgheib, N., & Balachandar, S. (2021). Peering inside a cough or sneeze to explain enhanced airborne transmission under dry weather. *Scientific Reports*, *11*(1), 1–9.

Liu, L., Li, Y., Nielsen, P.V., Wei, J., & Jensen, R.L. (2017). Short-range airborne transmission of expiratory droplets between two people. *Indoor Air*, *27*(2), 452–462. https://doi.org/10.1111/ina.12314

Marr, L.C., Tang, J.W., Van Mullekom, J., & Lakdawala, S.S. (2019). Mechanistic insights into the effect of humidity on airborne influenza virus survival, transmission and incidence. *Journal of the Royal Society Interface*, *16*(150), 20180298.

Matthews, T.G., Thompson, C.V., Wilson, D.L., Hawthorne, A.R., & Mage, D.T. (1989). Air velocities inside domestic environments: An important parameter in the study of indoor air quality and climate. *Environment International*, *15*, 545–550.

Moin, P., & Mahesh, K. (1998). Direct numerical simulation: A tool in turbulence research. *Annual Review of Fluid Mechanics*, *30*(1), 539–578.

Morawska, L., & Cao, J. (2020). Airborne transmission of SARS-CoV-2: The world should face the reality. *Environment International*, *139*(April), 105730. https://doi.org/10.1016/j.envint.2020.105730

Netz, R.R. (2020). Mechanisms of airborne infection via evaporating and sedimenting droplets produced by speaking. *The Journal of Physical Chemistry B*, *124*(33), 7093–7101.

Ng, C.S., Chong, K.L., Yang, R., Li, M., Verzicco, R., & Lohse, D. (2021). Growth of respiratory droplets in cold and humid air. *Physical Review Fluids*, *6*(5), 54303.

Nielsen, P.V., Olmedo, I., De Adana, M.R., Grzelecki, P., & Jensen, R.L. (2012). Airborne cross-infection risk between two people standing in surroundings with a vertical temperature gradient. *HVAC and R Research*, *18*(4), 552–561. https://doi.org/10.1080/10789669.2011.598441

Panchapakesan, N.R., & Lumley, J.L. (1993). Turbulence measurements in axisymmetric jets of air and helium. Part 1. Air jet. *Journal of Fluid Mechanics*, *246*, 197–223.

Patankar, S.V. (2018). *Numerical heat transfer and fluid flow*. CRC.

Pope, S.B. (2000). *Turbulent flows*. Cambridge, UK: Cambridge University Press.

Poydenot, F., Abdourahamane, I., Caplain, E., Der, S., Haiech, J., Jallon, A., . . . Andreotti, B. (2021). Risk assessment for long and short range airborne transmission of SARS-CoV-2, indoors and outdoors, using carbon dioxide measurements. *ArXiv*. Advance online publication. ArXiv:2106.09489.

Prather, B.K.A., Wang, C.C., & Schooley, R.T. (2020). Reducing transmission of SARS-CoV-2. *Science*, *368*(6498), 1422–1424. https://doi.org/10.1126/science.abc6197

Qian, H., & Li, Y. (2010). Removal of exhaled particles by ventilation and deposition in a multibed airborne infection isolation room. *Indoor Air*, *20*(4), 284–297. https://doi.org/10.1111/j.1600-0668.2010.00653.x

Ravichandran, S., Meiburg, E., & Govindarajan, R. (2020). Mammatus cloud formation by settling and evaporation. *Journal of Fluid Mechanics*, *899*, A27. https://doi.org/10.1017/jfm.2020.439

Ravichandran, S., & Narasimha, R. (2020). Non-precipitating shallow cumulus clouds: Theory and direct numerical simulation. *ArXiv*. Advance online publication. https://doi.org/10.48550/arXiv.2004.09631

Rosti, M.E., Cavaiola, M., Olivieri, S., Seminara, A., & Mazzino, A. (2021). Turbulence role in the fate of virus-containing droplets in violent expiratory events. *Physical Review Research*, *3*(1), 13091.

Rosti, M.E., Olivieri, S., Cavaiola, M., Seminara, A., & Mazzino, A. (2020). Fluid dynamics of COVID-19 airborne infection suggests urgent data for a scientific design of social distancing. *Scientific Reports*, *10*(1), 1–9.

Schuit, M., Ratnesar-Shumate, S., Yolitz, J., Williams, G., Weaver, W., Green, B., . . . Dabisch, P. (2020). Airborne SARS-CoV-2 is rapidly inactivated by simulated sunlight. *The Journal of Infectious Diseases*, *222*(4), 564–571.

Shao, S., Zhou, D., He, R., Li, J., Zou, S., Mallery, K., . . . Hong, J. (2021). Risk assessment of airborne transmission of COVID-19 by asymptomatic individuals under different practical settings. *Journal of Aerosol Science*, *151*(August 2020), 105661. https://doi.org/10.1016/j.jaerosci.2020.105661

Singhal, R., Ravichandran, S., Diwan, S.S., & Brown, G.L. (2021). Reynolds stress gradient and vorticity fluxes in axisymmetric turbulent jet and plume. In L. Venkatakrishnan, S. Majumdar, G. Subramanian, G. S. Bhat, R. Dasgupta, & J. Arakeri (Eds.), *Proceedings of 16th Asian Congress of Fluid Mechanics*. Singapore: Springer. https://doi.org/10.1007/978-981-15-5183-3

Smith, S.H., Somsen, G.A., van Rijn, C., Kooij, S., van der Hoek, L., Bem, R.A., & Bonn, D. (2020). Probability of aerosol transmission of SARS-CoV-2. *MedRxiv*. Advance online publication. https://doi.org/10.1101/2020.07.16.20155572

Sun, C.Bin, Wang, Y.Y., Liu, G.H., & Liu, Z. (2020). Role of the eye in transmitting human coronavirus. What we know and what we do not know. *Frontiers in Public Health*, *8*(April), 1–7. https://doi.org/10.3389/fpubh.2020.00155

Tan, Z.P., Silwal, L., Bhatt, S.P., & Raghav, V. (2021). Experimental characterization of speech aerosol dispersion dynamics. *Scientific Reports*, *11*(1), 1–12. https://doi.org/10.1038/s41598-021-83298-7

Tang, J.W., Liebner, T.J., Craven, B.A., & Settles, G.S. (2009). A schlieren optical study of the human cough with and without wearing masks for aerosol infection control. *Journal of the Royal Society Interface*, *6*(Suppl. 6), 727–736. https://doi.org/10.1098/rsif.2009.0295.focus

Turner, J.S. (1986). Turbulent entrainment: The development of the entrainment assumption, and its application to geophysical flows. *Journal of Fluid Mechanics*, *173*, 431–471.

US Department of Homeland Security (2020). *Estimated airborne decay of SARS-CoV-2* [Online calculator]. Retrieved from https://www.dhs.gov/science-and-technology/sars-airborne-calculator

Van Der Poel, E.P., Ostilla-Mónico, R., Donners, J., & Verzicco, R. (2015). A pencil distributed finite difference code for strongly turbulent wall-bounded flows. *Computers and Fluids*, *116*, 10–16.

Van Doremalen, N., Bushmaker, T., Morris, D.H., Holbrook, M.G., Gamble, A., Williamson, B.N., . . . Munster, V.J. (2020). Aerosol and surface stability of SARS-CoV-2 as compared with SARS-CoV-1. *New England Journal of Medicine*, *382*(16), 1564–1567.

Wang, J., Alipour, M., Soligo, G., Roccon, A., De Paoli, M., Picano, F., & Soldati, A. (2021). Short-range exposure to airborne virus transmission and current guidelines. *Proceedings of the National Academy of Sciences*, *118*(37), e2105279118.

Wei, J., & Li, Y. (2017). Human cough as a two-stage jet and its role in particle transport. *PloS ONE*, *12*(1), e0169235.

Wells, W.F. (1934). Droplets and Droplets nuclei. *American Journal of Epidemiology*, *20*(3), 611–618. https://doi.org/10.1093/oxfordjournals.aje.a118097

WHO Scientific Brief (2020, March 27). Modes of transmission of virus causing COVID-19: Implications for IPC precaution recommendations (Issue March). Retrieved from https://www.who.int/news-room/commentaries/detail/modes-of-transmission-of-virus-causing-covid-19-implications-for-ipc-precaution-recommendations

Wölfel, R., Corman, V.M., Guggemos, W., Seilmaier, M., Zange, S., Müller, M.A., . . . Wendtner, C. (2020). Virological assessment of hospitalized patients with COVID-2019. *Nature*, *581*(7809), 465–469. https://doi.org/10.1038/s41586-020-2196-x

Xie, H.-T., Jiang, S.-Y., Xu, K.-K., Liu, X., Xu, B., Wang, L., & Zhang, M.-C. (2020). SARS-CoV-2 in the ocular surface of COVID-19 patients. *Eye and Vision*, *7*(1), 7–9. https://doi.org/10.1186/s40662-020-00189-0

Yang, F., Pahlavan, A.A., Mendez, S., Abkarian, M., & Stone, H.A. (2020). Towards improved social distancing guidelines: Space and time dependence of virus transmission from speech-driven aerosol transport between two individuals. *Physical Review Fluids*, *5*(12), 1–10. https://doi.org/10.1103/PhysRevFluids.5.122501